



# In an Acidic Environment, Perimidin-10-one Derivatives were Evaluated as Potential Copper Corrosion Inhibitors (Experimental and Theoretical Examinations)

H. S. Gadow<sup>1</sup> · Thoraya A. Farghaly<sup>2,3</sup> · A. M. Eldesoky<sup>1,4</sup>

Received: 25 October 2021 / Revised: 16 February 2022 / Accepted: 21 February 2022 / Published online: 6 March 2022  
© The Author(s), under exclusive licence to Springer Nature Switzerland AG 2022

## Abstract

Some perimidin-10-one derivatives (**1–3**) were investigated for corrosion protection of copper in nitric acid solution 2.0 M using mass loss (ML), electrochemical frequency modulation (EFM), electrochemical impedance spectroscopy (EIS), and Tafel polarization techniques. At an optimum dose of  $1.1 \times 10^{-5}$  M, perimidin-10-one derivatives (**1–3**) provide 88.8% hindrance. These compounds were predominantly working as mixed inhibitors, according to Tafel. A corrosion hindrance mechanism was also devised using the EIS test. The Florry–Huggins isotherm governs the adsorption of perimidin-10-one derivatives (**1–3**) on the surface of Cu. The parameters of thermodynamic activation were estimated to build a corrosion hindrance mechanism. EDX and SEM were used to evaluate the morphology of protected copper. The results of experimental study were confirmed by theoretical analyses. The results of experimental study were confirmed by theoretical analyses. Quantum chemical calculations and molecular dynamic simulations have been used to apply theoretical studies. The low energy gap, mulliken, and fukui indices are all visible in quantum chemical computations. Compound **1** has a higher adsorption energy than the other compounds, according to the results of the molecular dynamics simulation. The following is the order in which the inhibition efficiency is regulated: (**1**) > (**2**) > (**3**).

---

✉ H. S. Gadow  
hsgado73@gmail.com

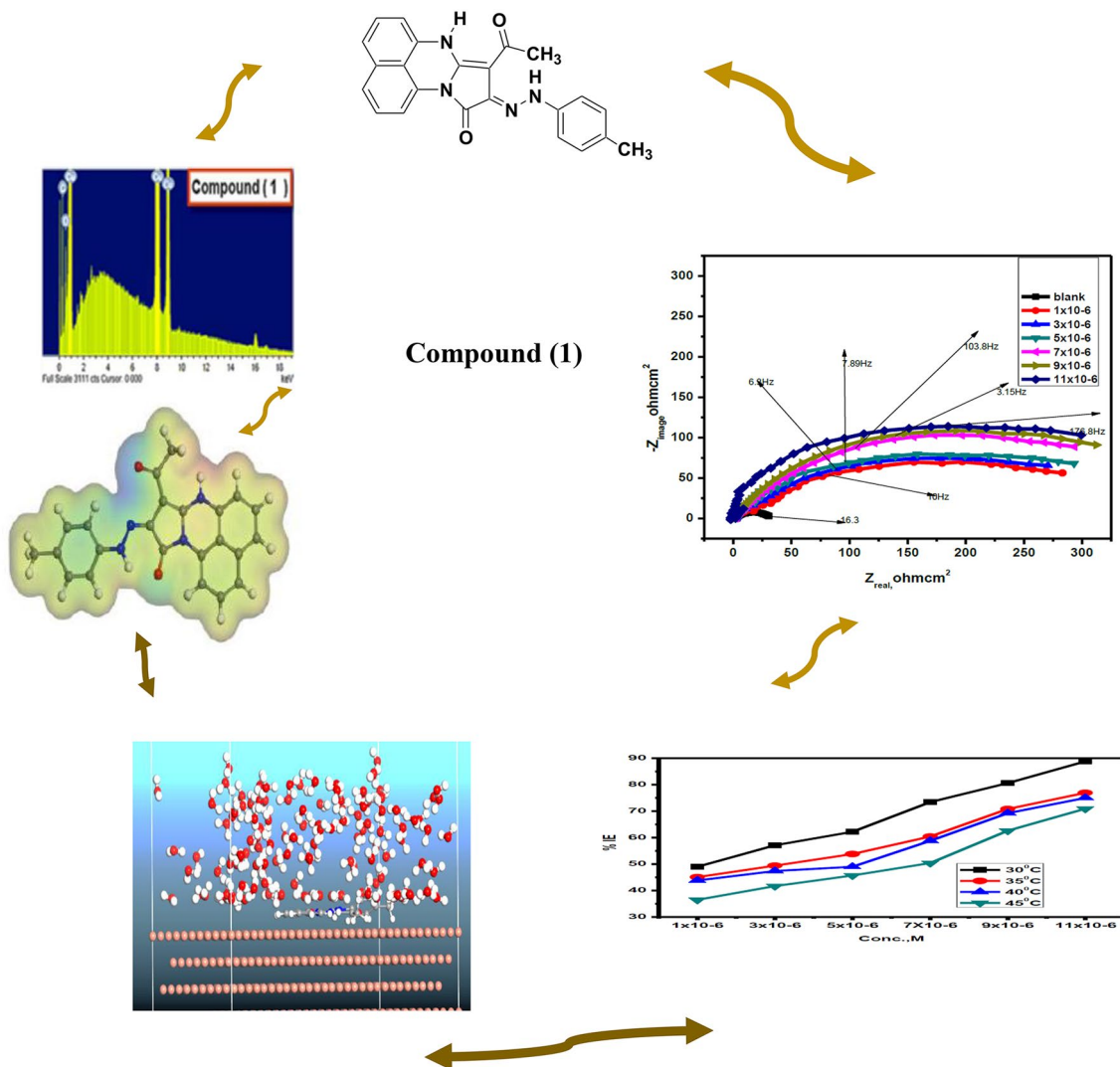
<sup>1</sup> Engineering Chemistry Department, Higher Institute for Engineering and Technology, New Demietta, New Damietta, Egypt

<sup>2</sup> Department of Chemistry, Faculty of Science, Cairo University, Giza 12613, Egypt

<sup>3</sup> Department of Chemistry, Faculty of Applied Science, Umm Al-Qura University, Makkah Almukkarramah, Saudi Arabia

<sup>4</sup> Al-Qunfudah Center for Scientific Research (QCSR), Chemistry Department, Al-Qunfudah University College, Umm Al-Qura University, Makkah Almukkarramah, Saudi Arabia

## Graphical Abstract



**Keywords** Copper · Corrosion inhibition · Electrochemical studies · Molecular dynamic studies

## 1 Introduction

Copper is utilized in a variety of electronic devices, including conductors, heat exchangers, and water pipelines; in addition, when used as a conductor in powerful electrical lines, it has a higher thermal and electrical conductivity. As a result, copper corrosion has been researched and settled in various solutions in multiple studies focusing on it [1–10]. For metallic copper, nitric acid is one of the most harmful corrosive conditions [11–16]. Corrosion yields have an inverse connection with heat transport. When the corrosion product grows, the equipment efficiency suffers. Periodic cleaning of equipment with acids is a vital step,

as corrosion develops when they come into contact [17]. Perimidin-10-one (1–3) products have a remarkable potential to delay corrosion due to the presence of heteroatoms in their molecules and are of particular interest due to their safe use and their large molecular size compared to other derivatives [13, 18–23]. Organic compounds with the elements “S, O, and N” with a heterocyclic structure have been utilized to prevent copper corrosion in water [24, 25]. Heterocyclic inhibitors with a mercapto group have been improved as copper inhibitors to prevent corrosion [26]. Cu-azole compounds are formed when nitrogen atoms engage with Cu via a lone pair of electrons in the azole compound [27]. These complexes are thought to be polymeric in nature and act as

a natural impediment coating on copper metals. Modified thiazole compounds [20, 28–34] have been calculated as effective inhibitors of copper alloys and copper corrosion in a varied aggressive environment.

The goal of this study is to investigate the effect of perimidin-10-one derivatives (1–3) as new copper corrosion inhibitors, and the adsorption approach was achieved using ML, electrochemical impedance spectroscopy (EIS), EFM, and TP techniques in a 2.0 M HNO<sub>3</sub> solution. Copper morphology was examined using SEM and EDX. In addition, theoretical investigations were used.

## 2 Techniques and Materials

### 2.1 The Chemical Makeup of Cu Samples

The copper utilized in this manuscript is composed of 0.001 Ni, 0.116 Si, 0.019 Al, 0.004 Mn, and the rest Cu (in wt%).

### 2.2 Solutions

In this investigation, we made a corrosive medium out of HNO<sub>3</sub> (6 M) made from 37 percent nitric acid analytical grade (Ramkem) and measured its concentration with a standardized NaOH. The concentrations of the three chemicals were increased from  $1 \times 10^{-6}$  to  $1.1 \times 10^{-5}$  M, and the weight-loss method and electrochemical studies employed 100 ml of test solution. Gomhoria Company provided absolute ethanol (EtOH, 99%), which was utilized to make an aqueous ethanol mixture with distilled water, which was used to make varied inhibitor doses. Because the inhibitors contain heteroatoms, they are easily dissolved.

### 2.3 The Chemical Composition of Perimidin-10-one Derivatives (1–3).

Table 1 shows the chemical makeup of the perimidin-10-one derivatives (1–3) employed in this study [35].

## 3 Experimental

### 3.1 ML Method

The Cu sample, which was  $2 \times 2 \times 0.2$  cm in size, was polished with sandpaper at various degrees (600, 800, 1000, and 1200). The sheet was cleaned with distilled water, removed with acetone, and dried according to industry standards [36]. Weight loss on the samples was measured after 30–180 min of treatment with varied doses of the selected inhibitor ( $1 \times 10^{-6}$ – $1.1 \times 10^{-5}$  M) at temperatures ranging from 30 to 45 °C using a water bath thermostat.

To acquire reliable findings, the experiment was repeated three times. To assess the difference between the presence and absence of various dosages of our examined compounds, the sample was weighed before being immersed in 100 ml of 2.0 M HNO<sub>3</sub> acid. The data of ML were obtained to calculate the CR in  $\text{mg}\cdot\text{cm}^{-2}\cdot\text{min}^{-1}$  by balance (1):

$$\text{Corrosion Rate (C.R.)} = \Delta W / At, \quad (1)$$

where  $A$  (area in  $\text{cm}^2$ ),  $t$  (time in min), and  $\Delta W$  (the mass difference). The inhibition efficacy (%IE) and ( $\theta$ ) were measured as follows:

$$\%IE = \text{Inhibition Efficiency} = [(M^* - M) / M^*] \times 100 = \theta \times 100, \quad (2)$$

where  $M$  and  $M^*$  are the amounts of copper corrosion in the presence and absence of the inhibitors, individually.

### 3.2 Tests of Electrochemical Studies

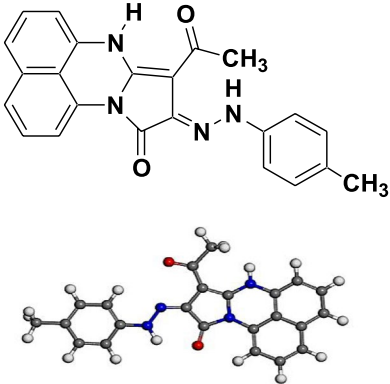
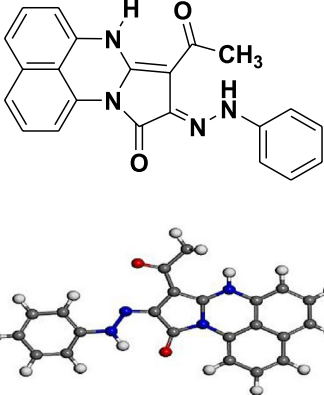
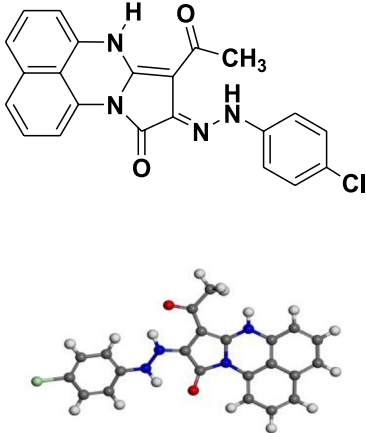
Gamry potentiostat/galvanostatic/ZRA (model PCI300/4) was used to make measurements at three derivative electrodes. Platinum foil was used as counter electrodes, SCE was used as a reference electrode, and the copper electrode was used as the working electrode ( $10 \times 10$  mm) and was welded from the first side by a copper wire that conducts electricity, and it's prepared the same way it was in the weight-loss approach previously. To stabilize the prior initial approach, the voltage for electrode use was acquired for 30 min. Tafel polarization curves for Perimidin-10-one derivatives (1–3) were generated by combining different electrode potentials ( $-300$  to  $+200$  mV) vs. OCP (a scan rate of  $1 \text{ mV s}^{-1}$ ).

Using the ESA400-based Gamry Frame System, the electrochemical frequency modulation (EFM) and EIS approaches were realized in the same way as before. The Gamry gadget comes with EFM140 software for electrochemical frequency adjustment testing and EIS300 software for electrochemical spectrum impedance method; data were collected using a computer. Drawing and fitting data have been done with Echem Analyst 5.5.

### 3.3 The Test of EDX-SEM

The surface of copper was accepted out by retaining the sheets for 3 days dipping in 2.0 M nitric acid in the presence or absence of higher dosages of perimidin-10-one derivatives (1–3), and then polishing mechanically with various papers emery up to 1600 size grit and treating them as weight-loss method sheets. The disadvantages of Cu were

**Table 1** Chemical composition of perimidin-10-one derivatives (1–3)

Compound no.	Name	Structure	Chemical formula and molecular weight
(1)	8-Acetyl-7H-9-(4-methyl phenyl hydrazono)-pyrrolo[1,2-a] perimidin-10-one		$C_{23}H_{18}N_4O_2$ (382.39)
(2)	8-Acetyl-7H-9-(phenyl hydrazono)-pyrrolo [1,2-a] perimidin-10-one		$C_{22}H_{16}N_4O_2$ (368.37)
(3)	8-Acetyl- 7H-9-(4-chlorophenyl hydrazono)-pyrrolo[1,2-a] perimidin-10-one		$C_{22}H_{15}N_4ClO_2$ (402.86)

explored using a Philips X-ray diffractometer (pw-1390) with a copper tube (“SEM, JSM-T20, JOEL, Japan”).

### 3.4 Quantum Measurements

PM3semi-empirical technique and density functional theory (DFT) were used to optimize our substances under

investigation. Materials Studio version 7 was used to do quantum chemical computations. The following equations were used to calculate the chemical parameters (electronegativity  $\chi$ , chemical potential  $P_i$ , and global hardness  $\eta$ ) [37, 38] using this method:

$$P_i = -\chi, \quad (3)$$

$$P_i = (E_{\text{LUMO}} + E_{\text{HOMO}})/2, \quad (4)$$

$$\eta = \Delta E/2 = (E_{\text{LUMO}} - E_{\text{HOMO}})/2. \quad (5)$$

By the global hardness, the softness is designated  $\sigma$ :

$$\sigma = 1/\eta. \quad (6)$$

The electronegativity and global hardness were used to compute the fraction of electrons transported ( $\Delta N$ ):

$$\Delta N = (\chi_{\text{Cu}} - \chi_{\text{inh}})/2(\eta_{\text{Cu}} - \eta_{\text{inh}}). \quad (7)$$

In the same order,  $\chi_{\text{inh}}$  and  $\chi_{\text{Cu}}$  denote the absolute electronegativity of inhibitor molecules and copper metal. According to Pearson's electronegativity scale, copper has an electronegativity of 4.48 and a hardness of 0 eV mol<sup>-1</sup> [39].

Furthermore, the local reactivity of a molecule was completed by Fukui function accounts. Fukui functions as the preferred sites for electrophilic and nucleophilic attacks of inhibitory molecules, respectively.

### 3.5 Molecular dynamics simulation

Molecular dynamic simulations (MD) were used in our study using Materials Studio version 7.0 and the adsorption Locator module [40]. The interaction between the copper (1 1 1) surface and the inhibitor molecules was molecular dynamically simulated using a simulation box (32.27 Å × 32.27 Å × 50.18 Å). The effect of any arbitrary barrier with occasional limit conditions is overridden to simulate a common section of the interface. MD computations were carried out using ten simulated annealing cycles (each with 1500 steps). Using the forcite classical emulation engine, the energy of molecules of examined derivatives was increased. The area of the copper (1 1 1) surface was increased, after which the copper surface (1 1 1) was organized by forming a supercell, the periodicity was adjusted, and a vacuum bulk with a density of 20 was applied to the copper (1 1 1) surface at that point [41]. After contracting the surface of copper (1 1 1) and the examined derivatives molecules, a layer builder was used to create the corrosion system. The compound molecules studied were deposited on the surface of copper (1 1 1), and the shrinking phase increased molecular potentials for the atomistic emulation calculated force field (COMPASS), on the copper (1 1 1) surface, which was employed to model the adsorption attitude for the molecules of the examined inhibitors. Through Monte Carlo analysis, the adsorption detector defines the

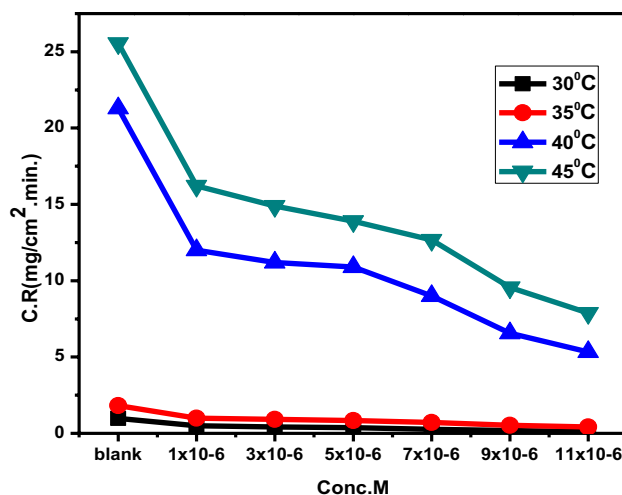


Fig. 1 The corrosion rate of several concentrations compound (1) on Cu in 2 M HNO<sub>3</sub> (30–45 °C)

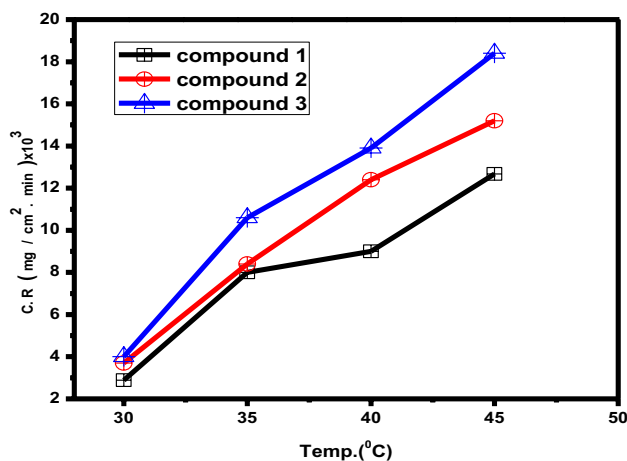


Fig. 2 Corrosion rate of three compounds ( $7 \times 10^{-6}$ ) on the surface of Cu in 2 M HNO<sub>3</sub> at 30–45 °C

way of adsorption arrangement for the examined chemicals molecules on the surface of copper (1 1 1). Furthermore, the adsorption modulation of our examined inhibitors, as well as its lack of influence on inhibition competence, was discovered [42]

## 4 Results and Discussion

### 4.1 ML Tests

Figure 1 shows the rate of copper corrosion in 2.0 M HNO<sub>3</sub> in the absence and presence of different dosages of compound (1) at 30–45 °C. By increasing the temperature, the inhibitory efficacy decreases and the corrosion rate

**Table 2** Data of ML of Cu in 2 M HNO<sub>3</sub> intended for various concentrations of derivative (1) after 90 min, at 30 and 35 °C

Conc. (M)	30 °C				35 °C			
	$\Delta W$ (mg cm <sup>-2</sup> )	$\theta$	%IE	C.R. (mg cm <sup>-2</sup> min <sup>-1</sup> × 10 <sup>3</sup> )	$\Delta W$ (mg cm <sup>-2</sup> )	$\theta$	%IE	C.R. (mg cm <sup>-2</sup> min <sup>-1</sup> × 10 <sup>3</sup> )
Blank	0.98 ± 0.0002			10.89	1.82 ± 0.0001			20.22
1 × 10 <sup>-6</sup>	0.50 ± 0.0001	0.490	49.0	5.56	1.0 ± 0.0003	0.451	45.1	11.11
3 × 10 <sup>-6</sup>	0.42 ± 0.0006	0.571	57.1	4.67	0.92 ± 0.0002	0.494	49.4	10.22
5 × 10 <sup>-6</sup>	0.37 ± 0.0003	0.622	62.2	4.11	0.84 ± 0.0004	0.538	53.8	9.33
7 × 10 <sup>-6</sup>	0.26 ± 0.0005	0.734	73.4	2.89	0.72 ± 0.0001	0.604	60.4	8.00
9 × 10 <sup>-6</sup>	0.19 ± 0.0002	0.806	80.6	2.11	0.53 ± 0.0002	0.708	70.8	5.89
11 × 10 <sup>-6</sup>	0.11 ± 0.0002	0.888	88.8	1.22	0.42 ± 0.0001	0.769	76.9	4.67

**Table 3** Data of ML of Cu in 2 M HNO<sub>3</sub> intended for various concentrations of derivative (1) after 90 min, at 40 and 45 °C

Conc. (M)	40 °C				45 °C			
	$\Delta W$ (mg cm <sup>-2</sup> )	$\theta$	%IE	C.R. (mg cm <sup>-2</sup> min <sup>-1</sup> × 10 <sup>3</sup> )	$\Delta W$ (mg cm <sup>-2</sup> )	$\theta$	%IE	C.R. (mg cm <sup>-2</sup> min <sup>-1</sup> × 10 <sup>3</sup> )
Blank	1.92 ± 0.0004			21.3	2.3 ± 0.0002			25.56
1 × 10 <sup>-6</sup>	1.08 ± 0.0005	0.438	43.8	12.0	1.46 ± 0.0004	0.365	36.5	16.22
3 × 10 <sup>-6</sup>	1.01 ± 0.0002	0.474	47.4	11.2	1.34 ± 0.0005	0.417	41.7	14.89
5 × 10 <sup>-6</sup>	0.98 ± 0.0003	0.490	49.0	10.9	1.25 ± 0.0004	0.457	45.7	13.89
7 × 10 <sup>-6</sup>	0.81 ± 0.0001	0.588	58.8	9.0	1.14 ± 0.0001	0.504	50.4	12.67
9 × 10 <sup>-6</sup>	0.59 ± 0.0003	0.692	69.2	6.56	0.86 ± 0.0001	0.626	62.6	9.56
11 × 10 <sup>-6</sup>	0.48 ± 0.0001	0.750	75.0	5.33	0.67 ± 0.0003	0.709	70.9	7.88

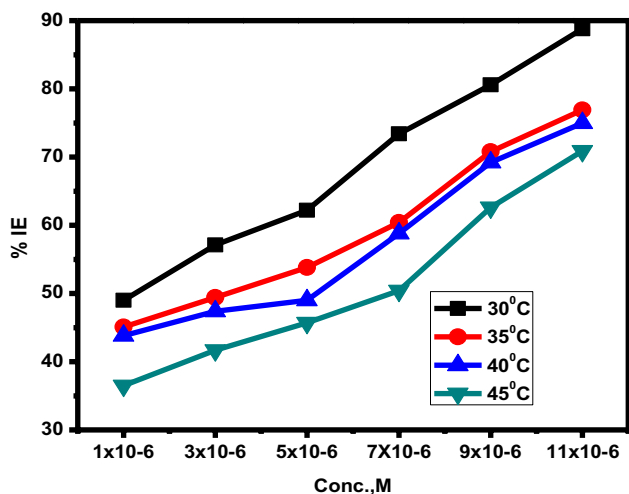


**Fig. 3** Variation of the inhibition efficiency of compound (1) at different concentrations on the surface of Cu in 2 M HNO<sub>3</sub> solution at 30–45 °C

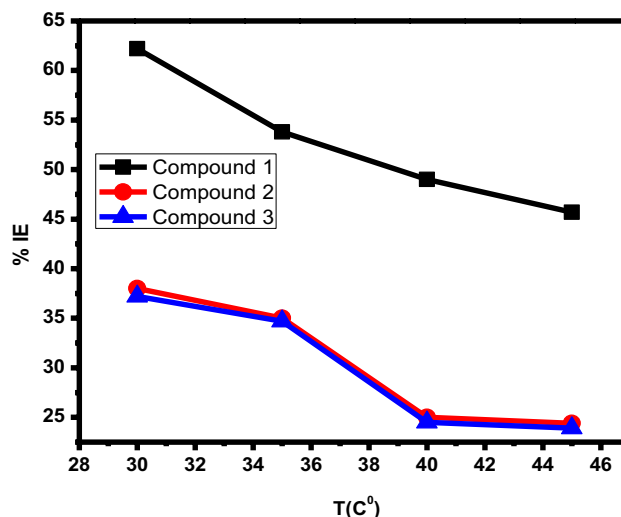


**Fig. 4** The inhibition efficiency variation of the three compounds (5 × 10<sup>-6</sup> M) on the surface of Cu in 2 M HNO<sub>3</sub> solution at 30–45 °C

increases. Because of the high temperature, the molecules of inhibitors are able to desorb from the copper surface at a consistent rate [43]. The corrosion rate of other studied compounds was found to be identical (not shown). Figure 2 shows a comparison of the corrosion rates of

different compounds at 7 × 10<sup>-6</sup>. According to the data in Tables 2, 3, and Fig. 3 for compound 1, the %IE increases as the dose increases from 1 × 10<sup>-6</sup> to 11 × 10<sup>-6</sup> molar and reduces as the temperature rises. For the remaining two

compounds, the same findings were achieved (not shown). At  $11 \times 10^{-6}$  molar, the good (%IE) was obtained. As a result, raising the concentration of our compounds leads to an increase in inhibitor molecule coverage on the copper surface [44]. Figure 4 compares the inhibitory efficiency of substances at different temperatures and at constant concentrations. The inhibition efficiency is organized in the following order: (1) > (2) > (3).

### 4.2 Adsorption Isotherm

The adsorption isotherm data are crucial for understanding the inhibitory corrosion mechanism in organic electrochemical reactions. The temperature of adsorption is influenced by a variety of factors. The nature and kind of metal surface, the structure of perimidin-10-one derivatives (1–3), the nature of the corrosion media, the electrochemical potential of the metal-solution interface, and temperature are all factors to consider. The adsorption isotherm should be estimated using the degree of surface covering ( $\theta$ ) of perimidin-10-one derivatives (1–3). Frumkin, Temkin, DeBoer, and other isotherms are among those used [45–49]. The slope values for the examined isotherms, as well as the computation of the regression coefficient ( $R^2$ ), are important factors to consider when choosing the best adsorption isotherms. The  $R^2$  value for the Florry Huggins isotherm was more exact than other isotherms because it was closer to the unit. Equation (8) is used to create this Florry Huggins isotherm, as seen in Fig. 5.

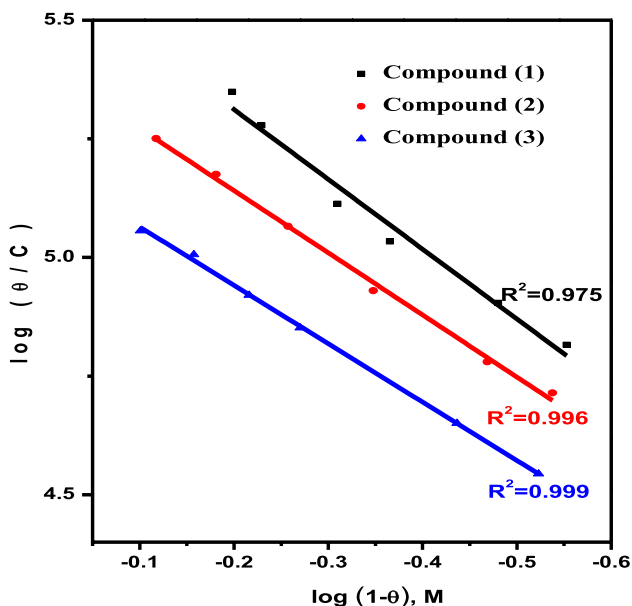


Fig. 5 Cu diagram of corrosion fitting data existence of altered doses of inhibitors follows Florry Huggins isotherm at  $30 \pm 1.0$  °C

$$\text{Log}\theta/C = \log xK_{\text{ads}} + x \log(1 - \theta) \tag{8}$$

When  $C$  is the inhibitor dose,  $K_{\text{ads}}$  is the adsorption equilibrium constant, the value of the size parameter  $x$  in  $\text{HNO}_3$  refers that the adsorbed inhibitors' molecules are bulky, where it could replace more than one water molecule from the copper surface. The highest  $K_{\text{ads}}$  data were found in compound 1, which has a higher IE than the other two compounds due to increased adsorption strength [50–52].

The equilibrium constant ( $K_{\text{ads}}$ ) of the adsorption technique can also be used to calculate ( $\Delta G_{\text{ads}}^\circ$ ) as a balance:

$$\Delta G_{\text{ads}}^\circ = -RT \ln (55.5K_{\text{ads}}), \tag{9}$$

where 55.5 is the water in the solution in M/L [53].

Table 4 shows the parameters collected from the adsorption technique. The negative data from  $\Delta G^\circ$  show that the pyrimidine-10-one derivatives (1–3) studied were substantially adsorbed on the copper surface, indicating a spontaneous process. The kind of adsorption is determined by the adsorption-free energy value; values of  $\Delta G_{\text{ads}}^\circ$  up to  $-20 \text{ kJ mol}^{-1}$  are consistent with physical adsorption, whereas those around  $-40 \text{ kJ mol}^{-1}$  or more are associated with chemisorption. The participation or transfer of electrons from molecules of perimidin-10-one derivatives (1–3) to the copper surface to form a coordinate bond is known as chemisorption [54]. The values of  $\Delta G_{\text{ads}}^\circ$  [15.19–15.11] in our study imply that physical adsorption is the major mode of perimidin-10-one derivatives (1–3) adsorption on the copper surface.

### 4.3 Kinetic–Thermodynamic Parameters

Arrhenius equation was used to compute the activation energies ( $E_a^*$ ) for copper corrosion in the absence and presence of a varied dose of perimidin-10-one derivatives (1–3) [55].

$$\log \text{C.R.} = \log A - E_a^*/2.303RT, \tag{10}$$

where  $A$  is the pre-exponential component. Figure 6 shows the Arrhenius bends of  $\log \text{C.R.}$  against  $1/T$  for Cu in 2.0 M

Table 4 Result got from Florry–Huggins isotherm ( $K_{\text{ads}}$ ), ( $\Delta G_{\text{ads}}^\circ$ ), and ( $x$ ) for inhibitors at 30 °C

Inhibitors	Florry–Huggins		
	$x$	$K_{\text{ads}} (\text{M}^{-1})$	$-\Delta G_{\text{ads}}^\circ (\text{kJ mol}^{-1})$
(1)	1.47	7.48	15.19
(2)	1.31	7.37	15.15
(3)	1.23	7.25	15.11

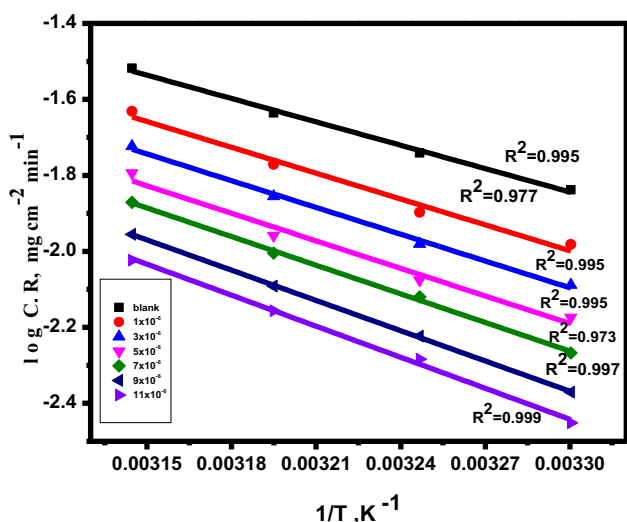


Fig. 6 Log C.R. vs. 1/T for Cu existence and nonexistence of altered doses of assembled (1)

Table 5 Parameters got from thermodynamic for the dissolution of Cu, an existence and nonexistence of altered doses of examined perimidin-10-one derivatives (1–3)

Inhibitor	Conc. (M)	$E_a^*$ (kJ mol <sup>-1</sup> )	$\Delta H^*$ (kJ mol <sup>-1</sup> )	$-\Delta S^*$ (J mol <sup>-1</sup> K <sup>-1</sup> )
Blank	–	39.25	38.13	154.66
(1)	1 × 10 <sup>-6</sup>	43.39	42.78	142.68
	3 × 10 <sup>-6</sup>	44.97	44.17	133.13
	5 × 10 <sup>-6</sup>	46.27	45.44	130.53
	7 × 10 <sup>-6</sup>	48.70	48.63	127.80
	9 × 10 <sup>-6</sup>	50.84	50.00	125.64
	11 × 10 <sup>-6</sup>	52.12	50.62	125.12
(2)	1 × 10 <sup>-6</sup>	42.54	41.69	145.43
	3 × 10 <sup>-6</sup>	43.74	45.55	134.33
	5 × 10 <sup>-6</sup>	45.26	46.68	131.82
	7 × 10 <sup>-6</sup>	46.48	47.90	129.11
	9 × 10 <sup>-6</sup>	48.86	48.68	128.48
	11 × 10 <sup>-6</sup>	50.75	49.81	126.02
(3)	1 × 10 <sup>-6</sup>	40.79	40.43	148.79
	3 × 10 <sup>-6</sup>	42.63	43.32	140.94
	5 × 10 <sup>-6</sup>	44.08	45.69	134.38
	7 × 10 <sup>-6</sup>	44.69	46.91	131.37
	9 × 10 <sup>-6</sup>	47.43	47.58	130.47
	11 × 10 <sup>-6</sup>	49.55	49.63	125.65

HNO<sub>3</sub> acid in nonexistence and an existence-altered dose of (1). Table 5 shows the  $E_a^*$  data, which were calculated from the slope of these lines. The  $E_a^*$  value greater than 20 kJ mol<sup>-1</sup> was used to determine whether physisorption occurred in the first step [56]. Equation (11) [57] is used to calculate ( $\Delta S^*$ ,  $\Delta H^*$ ) for Cu corrosion in HNO<sub>3</sub> solution:

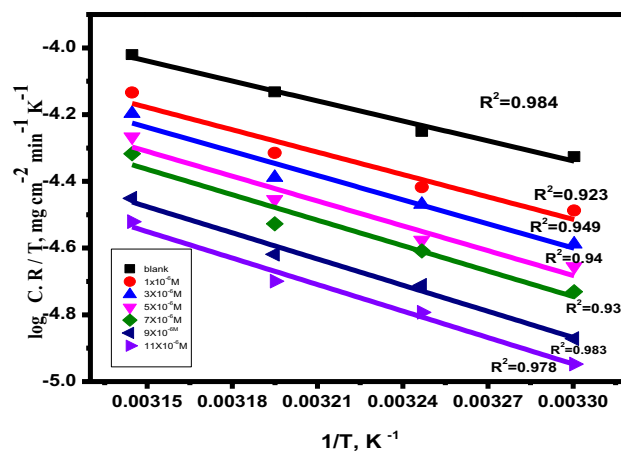
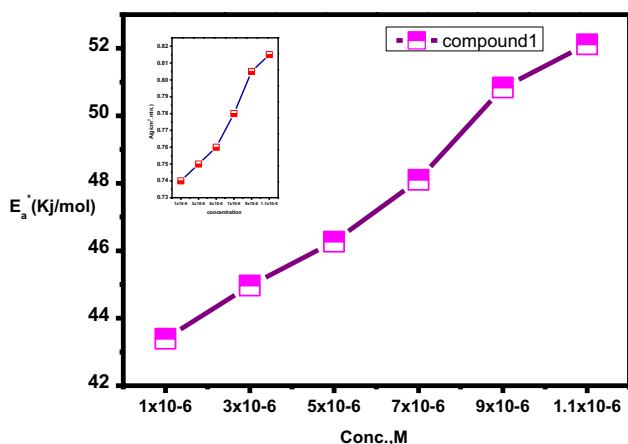


Fig. 7 Transition state bends for Cu existence and nonexistence of altered doses of assembled (1)

$$C.R. = (TR/Nh) e (\Delta S^*/R) e (-\Delta H^*/RT). \tag{11}$$

Planck’s constant is denoted by  $h$ . A plot of  $\log C.R./T$  against  $1/T$  produced linear lines for Cu in 2.0 M HNO<sub>3</sub> acid nonexistence and the presence of changed dose, as illustrated in Fig. 7. Table 5 shows the results of the  $\Delta H^*$  and  $\Delta S^*$  calculations. The endothermic process was approximated using the +ve sign of the  $\Delta H^*$  [58]. Table 5 shows that the activation energy for a blank solution is 39.25 kJ mol<sup>-1</sup>, and that this activation energy value for copper corrosion in 2.0 M HNO<sub>3</sub> is in good accord with other studies [59]. In the presence of perimidine-10-one derivatives, the activation energy increases (1–3). The nature of their adsorption on the copper surface is attributed to the higher rate of  $\Delta E_a^*$  in the presence of three derivatives [60–63]. This observation demonstrates that physisorption is used in the adsorption process [64, 65]. The greater energy barrier was responsible for the higher value of  $E_a$  in the presence of three inhibitors. This occurrence also supports the existence of a complex compound between the inhibitor and copper [65]. Because of the increased energy barrier for metal dissolving, these data show that the inhibitors can limit corrosion. The creation of a thin coating on the copper surface acts as an energy and mass transfer barrier, raising the activation energy. As a result, the finding indicates that inhibitors’ adsorption on copper is due to physical adsorption. The activation energy increased as the inhibitor concentration increased, as seen in the tables. The activation energy was, however, still larger than in the uncontrolled solution. These findings are consistent with those of prior studies [66–69]. The variation in pre-exponential factor ( $A$ ) was found to be similar to that in apparent activation energy in both acids (see Fig. 8). Some researchers had reported similar outcomes [70–72]. Greater pre-exponential variables were shown to be linked with





**Fig. 8** The relation of  $E_a^*$  and  $A$  with the concentration of compound 1 2.0 M  $\text{HNO}_3$

higher apparent activation energies in the current investigation, whereas lower pre-exponential factors were found to be associated with lower activation energies. As a result, even at the lowest corrosion activation energies, the tested inhibitor showed good inhibitive properties. All values of  $E_a^*$  are greater than equivalent values of  $\Delta H^*$  in both acids, indicating that the corrosion process must involve a gaseous reaction, such as hydrogen evolution. Furthermore, the average value of the difference between activation energy and enthalpy is approximately similar to the average value of  $RT$ , where  $T$  is in the range of the experimental temperatures, indicating that the corrosion process is a uni-molecular reaction as defined by Eq. 12 [73]:

$$E_a - \Delta H^* = RT. \quad (12)$$

The  $\Delta S^*$  data at the existence and nonexistence of the tested compounds are maximal and  $-ve$  sign; i.e., the activated complex favors association over dissociation in the rate-determining phase, implying that there is less disordering [74, 75].

## 5 Potentiodynamic Polarization Tests

In order to gather knowledge, potentiodynamic polarization looked into the kinetics of cathodic and anodic reactions. The potentiodynamic polarization technique of Cu in 2 M  $\text{HNO}_3$  solution is illustrated in Fig. 9 in the presence and absence of various dosages of perimidin-10-one derivatives (1). (Other compounds yielded similar findings; however, they were not presented). The extra doses of chemical 1 resulted in this graph, which demonstrated that. When compared to the blank curve, the Tafel lines have moved to become more

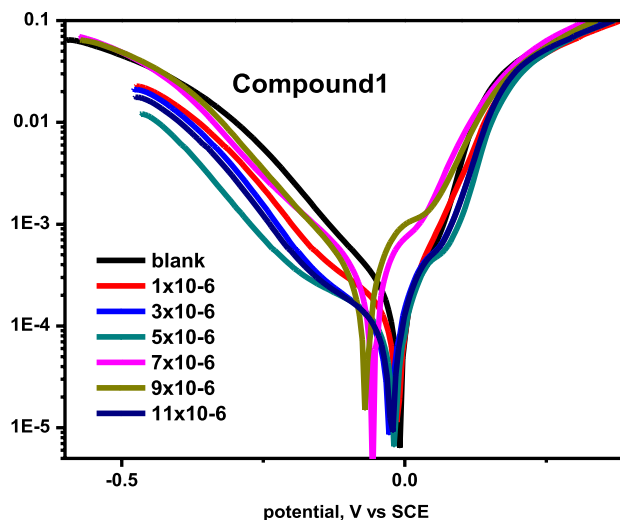


**Fig. 9** Potentiodynamic polarization bends for the Cu corrosion in the presence and absence of altered doses of derivative (1) at  $30 \pm 1.0$  °C

positive and negative potentials, indicating that perimidin-10-one derivatives (1–3) are active mixed-type inhibitors [76–78]. Table 6 shows the findings of potentiodynamic polarization [corrosion potential ( $E_{\text{corr}}$ ), corrosion current density ( $i_{\text{corr}}$ ), and corrosion inhibition (%IE)] [anodic and cathodic Tafel constants ( $\beta_a$  and  $\beta_c$ ) correspondingly, corrosion potential ( $E_{\text{corr}}$ ), corrosion current density ( $i_{\text{corr}}$ ), and corrosion inhibition (%IE)]. Table 6 shows that increasing the quantities of our examined chemicals (perimidin-10-one derivatives) causes a modest alteration in the cathode and anodic Tafel slopes (1–3). This suggests that the inhibitory mechanism is unaffected by the presence or absence of our derivatives on cathode and anode reactions [79, 80]. The minimal variance in  $E_{\text{corr}}$  data suggests that the chemicals studied are mixed-type inhibitors [81–83]. Copper metal is easily oxidized in nitric acid solutions because nitric acid is a powerful oxidant of copper. The Pourbaix scheme of the copper–water system [84, 85] demonstrated that in nitric acid solutions, copper metal corrosion to  $\text{Cu}^{+2}$  occurs and that the copper surface is not shielded by an oxide film [86]. In nitric acid solutions, copper degradation is thought to be the dominating process. The results of potentiodynamic polarization (Table 6) show that attendance inhibitors reduce  $i_{\text{corr}}$  and that the %IE increases as the dose is increased. The following equation was used to compute the percentage IEp:

$$\%IEp = 100 \times [(i_{\text{corr}}^{\circ} - i_{\text{corr}}) / i_{\text{corr}}^{\circ}], \quad (13)$$

where the currents of corrosion presence and nonexistence, respectively, are  $i_{\text{corr}}^{\circ}$  and  $i_{\text{corr}}$ . Increasing the dosage of adsorbed derivatives on the copper surface increases polarization resistance (Fig. 10) [87].

**Table 6** Potentiodynamic polarization parameters ( $E_{corr}$ ), ( $i_{corr}$ ), ( $\beta_a$  and  $\beta_c$ ), ( $\theta$ ), and (%IE) for Cu in HNO<sub>3</sub> (2.0 M) at 30 ± 1.0 °C

Inhibitor	Conc. (M)	$-E_{corr}$ (mV vs. SCE)	R ( $\Omega$ )	$i_{corr}$ ( $\mu\text{A cm}^{-2}$ )	$-\beta_a \times 10^3$ (V dec <sup>-1</sup> )	$-\beta_c \times 10^3$ (V dec <sup>-1</sup> )	$\theta$	%IEp
Blank	Blank	9.25 ± 0.3	2.48 ± 0.1	414.00 ± 8	101.9 ± 2	215.9 ± 4	–	–
(1)	1 × 10 <sup>-6</sup>	12.60 ± 0.2	10.38 ± 0.2	271.20 ± 2	90.5 ± 3	193.7 ± 2	0.345	34.5
	3 × 10 <sup>-6</sup>	17.40 ± 0.1	11.43 ± 0.1	226.87 ± 3	84.9 ± 1	194.3 ± 3	0.452	45.2
	5 × 10 <sup>-6</sup>	23.50 ± 0.2	11.86 ± 0.2	127.93 ± 2	81.6 ± 2	197.1 ± 4	0.691	69.1
	7 × 10 <sup>-6</sup>	34.50 ± 0.4	13.20 ± 0.1	84.87 ± 3	116.0 ± 5	182.9 ± 2	0.795	79.5
	9 × 10 <sup>-6</sup>	23.60 ± 0.2	15.30 ± 0.3	69.97 ± 2	122.0 ± 3	188.5 ± 4	0.831	83.1
	11 × 10 <sup>-6</sup>	9.40 ± 0.1	15.79 ± 0.1	64.99 ± 3	80.5 ± 0.8	184.7 ± 3	0.843	84.3
(2)	1 × 10 <sup>-6</sup>	9.27 ± 0.05	6.58 ± 0.2	281.10 ± 5	112 ± 0.9	199.2 ± 5	0.321	32.1
	3 × 10 <sup>-6</sup>	9.30 ± 0.2	9.26 ± 0.1	256.68 ± 4	85 ± 2	199.6 ± 2	0.380	38.0
	5 × 10 <sup>-6</sup>	16.00 ± 0.3	9.86 ± 0.05	153.60 ± 2	89 ± 0.7	231.0 ± 6	0.629	62.9
	7 × 10 <sup>-6</sup>	26.80 ± 0.1	12.71 ± 0.05	114.30 ± 3	122 ± 2	216.8 ± 5	0.724	72.4
	9 × 10 <sup>-6</sup>	13.50 ± 0.3	13.73 ± 0.2	92.32 ± 0.9	116 ± 3	195.4 ± 3	0.777	77.7
	11 × 10 <sup>-6</sup>	34.20 ± 0.2	14.85 ± 0.3	87.35 ± 1	113 ± 4	197.5 ± 2	0.789	78.9
(3)	1 × 10 <sup>-6</sup>	15.40 ± 0.1	6.14 ± 0.4	293.11 ± 7	81.2 ± 2	198.6 ± 3	0.292	29.2
	3 × 10 <sup>-6</sup>	10.60 ± 0.2	7.34 ± 0.2	267.03 ± 4	106.4 ± 5	218.9 ± 6	0.355	35.5
	5 × 10 <sup>-6</sup>	9.31 ± 0.1	9.04 ± 0.1	240.95 ±	92.4 ± 2	196.2 ± 3	0.418	41.8
	7 × 10 <sup>-6</sup>	7.20 ± 0.05	10.68 ± 0.03	183.40 ±	95.3 ± 0.7	209.6 ± 7	0.557	55.7
	9 × 10 <sup>-6</sup>	13.30 ± 0.1	11.27 ± 0.06	130.41 ±	84.1 ± 0.8	199.8 ± 3	0.685	68.0
	11 × 10 <sup>-6</sup>	26.80 ± 0.2	12.07 ± 0.2	95.63 ±	86.3 ± 0.5	148.6 ± 2	0.769	76.9

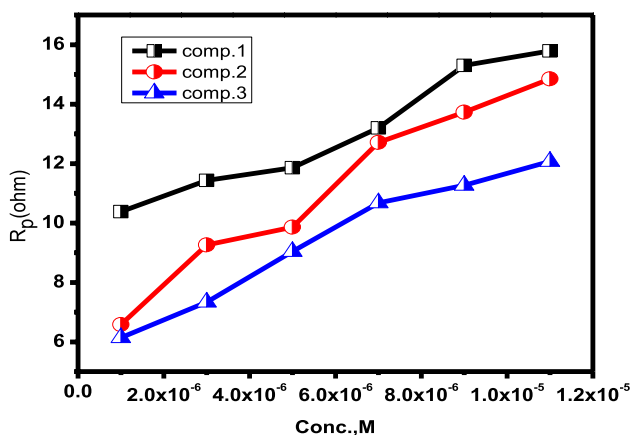


**Fig. 10** Polarization resistance for the copper corrosion in present and nonexistence of altered doses of studied derivatives at 30 ± 1.0 °C

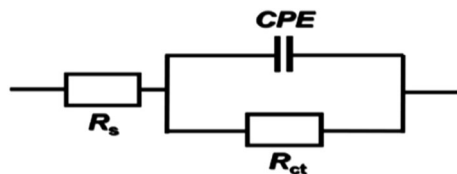


**Fig. 11** Equivalent circuit utilized to fit result EIS

The %IEP of these perimidin-10-one derivatives (1–3) is as follows: (1) > (2) > (3).

### 5.1 EIS Tests

In the manuscript of corrosion, EIS is a powerful method [88–92]. The values of impedance for a copper electrode were calculated using the equivalent circuit shown in Fig. 11 in the presence of various concentrations of our derivatives. Instead of capacitors, this circuit uses constant phase elements (CPE) to simulate a variety of non-homogeneities that cause electrode corrosion, including as insufficient polishing, surface roughness, grain boundaries, and surface contaminants [93]. In our examination of the arithmetic expression on the frequency, we employed two parameters ( $Y^0$  and  $n$ ), with the impedance of copper dependent on this frequency being observed in the following equation [94].

$$Z_{CPE} = Y^{0-1} (j\omega)^{n-1}. \tag{14}$$

The CPE coefficient was represented by the symbol  $Y^0$  in the equation, whereas the sine wave angular frequency and imaginary number were represented by the letters  $\omega$  and  $j^2 = -1$ . Given  $2\pi f$  as a character  $\omega$ , where  $f$  is the sign for AC frequency. The  $n$  ideals in real investigative settings are between 0 and 1, for a variety of reasons, including electrode roughness, constant electrical insulation, and surface

heterogeneity. When the  $n$  values of the inhibition system were compared to the  $n$  values of 2 M HNO<sub>3</sub> as a blank in this study, we discovered that the copper surface in the inhibition system is relatively more homogeneous, which is due to the regularity of adsorption for perimidin-10-one derivatives (1–3) molecule on the surface of copper [95]. The following equation showed how to compute the capacitance of a double layer ( $C_{dl}$ ) [96]:

$$C_{dl} = Y^0 \omega^{n-1} / \sin[n(\pi/2)]. \tag{15}$$

In our investigation, we used the following Eq. [97] to calculate the surface coverage degree ( $\theta$ ) and inhibition efficiency (%IE):

$$\%IE = \theta \times 100 = [1 - (R_{ct}^0/R_{ct})] \times 100. \tag{16}$$

The impedance of charge transport without and with derivatives was investigated and expressed as  $R_{ct}^0$  and  $R_{ct}$ , respectively. As a result of the interface between the copper surface and the aqueous electrolyte, a line of ions (both positively and negatively charged) forms. Furthermore, it protects the surface by coating or forming a film. Capacitance is determined by the electrical double layer ( $C_{dl}$ ), solution resistance ( $R_s$ ), charge transfer resistance ( $R_{ct}$ ), and ion diffusion. The movement of charge in or away from the copper surface causes a wide range of impedances, as does the adsorption of cations and anions. Table 7 shows the copper impedance parameters in 2 M HNO<sub>3</sub> without

and with the addition of various amounts of the chemicals studied. Figures 12 and 13 show charts obtained from [Nyquist and Bode] for copper in the presence of various amounts of the chemicals investigated (other compounds not shown). The diameter of the semicircle grows as the concentration of the examined substances increases, as seen in Fig. 12. As a result, the corrosion process experiences an increase in transfer resistance. As a result of the strong resistance displayed by the adsorbent molecules of the compounds studied at the copper alloy/solution interface [98], this is the case. Nyquist plots did not close as expected in our investigation, indicating a divergence from the EIS theory. Due to the heterogeneity of the copper surface and frequency dispersion, the aberration is from the ideal semicircle [99]. Different concentrations of different derivatives result in a drop in  $C_{dl}$  when compared to the blank solution by decreasing the local dielectrical constant and/or increasing the thickness of the double electric layer. The adsorption of pyrimidine-10-derivative molecules (1–3) in the copper/solution contact is responsible for this [100, 101]. Impedance charts have a semi-circular appearance, indicating the charge transfer mechanism, which is primarily responsible for controlling copper corrosion [102, 103]. The rise of impedance data in the presence of the inhibitors investigated is two-fold higher than in the absence of them, as seen in the Bode graphs in Fig. 13, showing the observed corrosion inhibition of the three inhibitors studied. Furthermore, as the frequency range

**Table 7** EIS parameters for Cu nonexistence and existence-altered doses of perimidin-10-one derivatives (1–3) at 30 ± 1.0 °C

Inhibitor	Conc. (M)	RS (Ω cm <sup>2</sup> )	Y <sup>0</sup> × 10 <sup>6</sup> (μΩ <sup>-1</sup> sn)	n × 10 <sup>3</sup>	R <sub>ct</sub> (Ω cm <sup>2</sup> )	C <sub>dl</sub> × 10 <sup>-4</sup> (μF cm <sup>-2</sup> )	θ	%IE
Blank	Blank	1.500 ± 0.015	260.4 ± 3.4	624.0 ± 2.5	29.76 ± 0.025	5.57	–	–
(1)	1 × 10 <sup>-6</sup>	1.790 ± 0.016	533.7 ± 3.6	742.7 ± 3.4	289.2 ± 3.1	2.79	0.897	89.7
	3 × 10 <sup>-6</sup>	1.855 ± 0.017	625.3 ± 4.6	726.7 ± 3.2	300.2 ± 3.3	2.68	0.901	90.1
	5 × 10 <sup>-6</sup>	1.645 ± 0.015	559.1 ± 3.9	707.8 ± 2.9	303.5 ± 3.5	2.64	0.902	90.2
	7 × 10 <sup>-6</sup>	1.660 ± 0.016	708.1 ± 5.3	713.3 ± 3.1	307.6 ± 3.7	2.29	0.903	90.3
	9 × 10 <sup>-6</sup>	1.627 ± 0.013	705.7 ± 5.1	727.0 ± 3.7	319.2 ± 3.9	2.28	0.907	90.7
	11 × 10 <sup>-6</sup>	1.878 ± 0.016	568.4 ± 4.1	709.0 ± 3.1	346.5 ± 4.1	1.77	0.914	91.4
(2)	1 × 10 <sup>-6</sup>	1.886 ± 0.014	954.9 ± 7.5	679.5 ± 2.8	200.4 ± 2.5	3.84	0.852	85.2
	3 × 10 <sup>-6</sup>	1.559 ± 0.015	857.3 ± 6.4	734.4 ± 3.8	203.8 ± 2.6	3.53	0.854	85.4
	5 × 10 <sup>-6</sup>	1.601 ± 0.017	830.5 ± 6.1	717.7 ± 3.5	213.3 ± 2.4	3.45	0.860	86.0
	7 × 10 <sup>-6</sup>	1.661 ± 0.016	396.9 ± 3.8	746.2 ± 3.9	235.3 ± 2.6	3.40	0.874	87.4
	9 × 10 <sup>-6</sup>	1.560 ± 0.016	465.9 ± 3.7	749.0 ± 3.9	257.8 ± 2.7	3.24	0.885	88.5
	11 × 10 <sup>-6</sup>	1.808 ± 0.017	544.7 ± 3.9	720.8 ± 3.6	284.3 ± 2.8	2.91	0.895	89.5
(3)	1 × 10 <sup>-6</sup>	1.629 ± 0.016	848.4 ± 6.2	769.9 ± 2.8	141.2 ± 1.7	4.82	0.789	78.9
	3 × 10 <sup>-6</sup>	1.627 ± 0.015	984.8 ± 7.9	757.3 ± 3.9	149.0 ± 1.8	4.37	0.800	80.0
	5 × 10 <sup>-6</sup>	1.883 ± 0.017	926.9 ± 7.2	746.5 ± 3.8	157.5 ± 1.9	4.34	0.811	81.1
	7 × 10 <sup>-6</sup>	1.956 ± 0.018	101.1 ± 3.4	759.9 ± 3.7	170.0 ± 2.1	4.20	0.825	82.5
	9 × 10 <sup>-6</sup>	1.878 ± 0.017	553.1 ± 6.1	724.4 ± 3.6	178.8 ± 2.2	4.11	0.834	83.4
	11 × 10 <sup>-6</sup>	1.723 ± 0.017	753.8 ± 6.5	700.6 ± 3.5	184.4 ± 2.4	4.07	0.839	83.9

**Fig. 12** EIS Nyquist curves for Cu surface without and with of altered doses of composite (1) at  $30 \pm 1$  °C

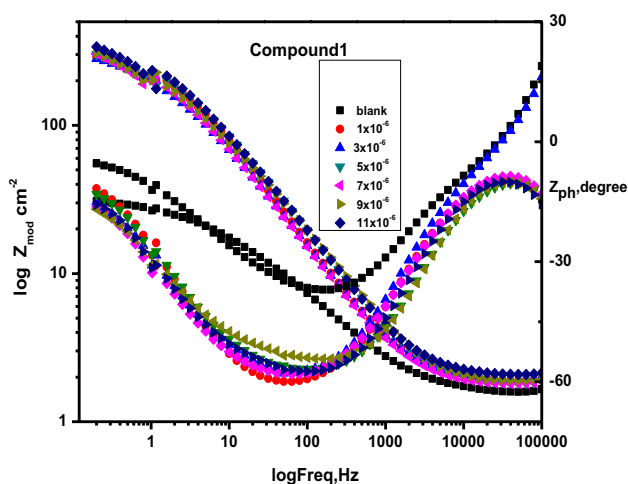
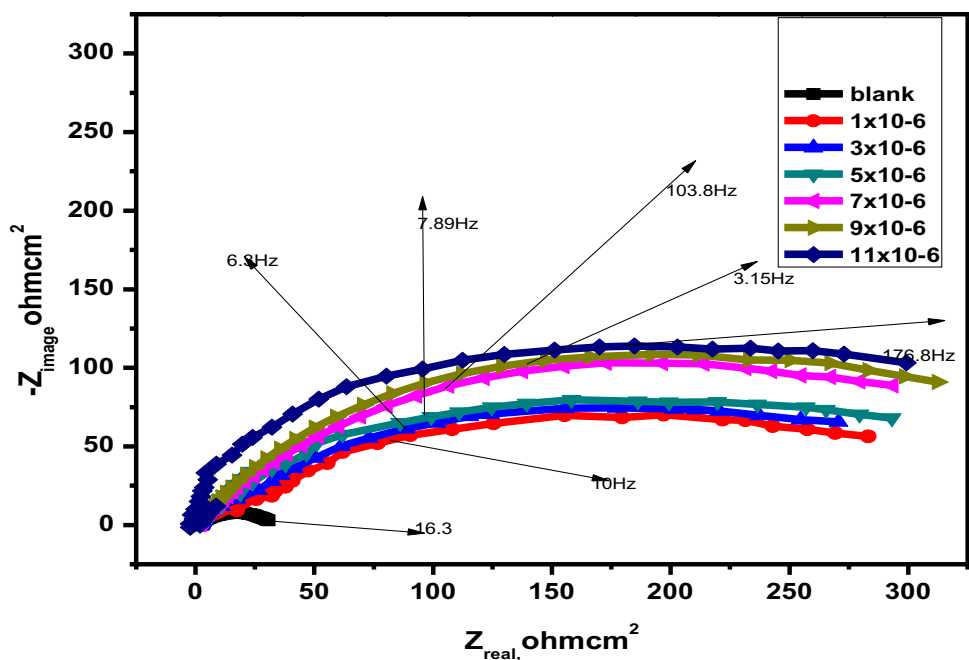


**Fig. 13** EIS Bode curves for Cu surface without and with of altered doses of composite (1) at  $30 \pm 1$  °C

widens due to higher inhibitor concentrations, the maximum phase angle reveals the real adsorption of compounds molecules on the copper surface. In the corrosion probability,  $E_{corr}$ , spectroscopy of electrochemical resistance was explored throughout a frequency range of 105 Hz to 0.1 Hz and discomfort with a signal capacity of 10 mV. Ranking of %IE: (1) > (2) > (3).

### 5.2 EFM Tests

Without previous data from the Tafel slopes, EFM is a safe corrosion screening approach that can withstand and

evaluate the value of present corrosion quickly [104]. Causal factors appear to be an internal survey on EFM test precision [105]. The frequency spectrum stream is used to calculate CF-2 and CF-3. This approach contains a little AC signal, similar to the EIS method, but there is a difference between the two methods since EFM uses two sine waves (at different frequencies) in the cell at the same time. Because current is a nonlinear function of potential, the system reacts to potential excitement in a nonlinear manner. There are input frequencies and frequency components in the current response (difference, total, input frequency multipliers). To establish the length of the test, these frequencies must be modest and integer multiples of the base frequency. Table 8 contains a list of corrosion parameters. Table 8 shows that the measured values of causation factors are of good quality. CF-2 and CF-3 have regular values of 2.0 and 3.0, respectively. When the values of causality factors deviate from the conventional values, it means that the measured values are influenced by noise. There is a causal connection between the response signal and the perturbation signal when the experimental values and theoretical values for causality factors agree. The data should, thus, be trustworthy [106]. We discovered that as we increased the doses of our compounds, the current corrosion intensity decreased (Fig. 14). Simultaneously, the efficiency of inhibition of the investigated compounds improves. The inhibitory efficiency of this approach was estimated using the equation below.

$$\%IE_{EFM} = \theta \times 100 = 100 \times [1 - (i_{corr}/i_{corr}^{\circ})]. \quad (17)$$

**Table 8** EFM data gotten for Cu nonexistence and an existence-altered doses of perimidin-10-one derivative (1–3) at  $30 \pm 1.0$  °C

Inhibitor	Conc. (M)	$i_{\text{corr}}$ ( $\mu\text{A cm}^{-2}$ )	$\beta_a \times 10^{-3}$ (mV dec $^{-1}$ )	$\beta_c \times 10^{-3}$ (mV dec $^{-1}$ )	CF-2	CF-3	$\theta$	%IE <sub>EFM</sub>	C.R. mpy
Blank	Blank	514.00 ± 8	105.80 ± 2	118.0 ± 2	1.96 ± 0.04	3.08 ±	–	–	234.9
(1)	1 × 10 $^{-6}$	74.45 ± 2	57.49 ± 0.4	159.7 ± 3	1.87 ± 0.03	2.75 ± 0.01	0.855	85.5	44.48
	3 × 10 $^{-6}$	73.42 ± 3	59.30 ± 0.7	151.9 ± 1	1.94 ± 0.02	3.34 ± 0.02	0.857	85.7	43.31
	5 × 10 $^{-6}$	72.35 ± 1	61.21 ± 0.9	169.5 ± 3	1.85 ± 0.02	3.07 ± 0.04	0.859	85.9	42.68
	7 × 10 $^{-6}$	69.33 ± 0.5	66.16 ± 0.4	195.1 ± 2	1.92 ± 0.05	3.41 ± 0.03	0.865	86.5	40.9
	9 × 10 $^{-6}$	63.51 ± 0.7	62.79 ± 0.7	207.9 ± 3	1.95 ± 0.03	3.07 ± 0.02	0.876	87.6	31.34
	11 × 10 $^{-6}$	60.97 ± 0.5	52.38 ± 0.5	108.0 ± 2	1.84 ± 0.03	3.03 ± 0.03	0.881	88.1	30.09
(2)	1 × 10 $^{-6}$	102.20 ± 2	54.55 ± 0.4	133.2 ± 4	1.96 ± 0.03	3.06 ± 0.05	0.801	80.1	60.27
	3 × 10 $^{-6}$	90.92 ± 0.2	52.93 ± 0.6	122.4 ± 2	1.91 ± 0.02	3.04 ± 0.02	0.823	82.3	48.87
	5 × 10 $^{-6}$	84.99 ± 2	63.13 ± 0.3	63.1 ± 0.8	1.87 ± 0.04	3.23 ± 0.03	0.835	83.5	44.77
	7 × 10 $^{-6}$	82.88 ± 1	57.91 ± 0.6	137.3 ± 3	1.90 ± 0.05	3.30 ± 0.02	0.839	83.9	44.55
	9 × 10 $^{-6}$	81.63 ± 0.9	56.21 ± 0.2	168.6 ± 3	1.97 ± 0.03	3.22 ± 0.04	0.841	84.1	38.84
	11 × 10 $^{-6}$	75.52 ± 0.8	59.79 ± 0.3	186.6 ± 4	1.95 ± 0.02	3.03 ± 0.02	0.853	85.3	37.30
(3)	1 × 10 $^{-6}$	182.50 ± 3	49.81 ± 0.5	118.9 ± 2	1.88 ± 0.04	3.04 ± 0.04	0.645	64.5	107.6
	3 × 10 $^{-6}$	173.40 ± 4	55.72 ± 0.6	152.9 ± 3	1.92 ± 0.05	2.81 ± 0.05	0.663	66.3	102.3
	5 × 10 $^{-6}$	136.20 ± 2	53.92 ± 0.2	140.5 ± 0.9	1.93 ± 0.03	2.92 ± 0.02	0.735	73.5	79.18
	7 × 10 $^{-6}$	134.20 ± 3	55.49 ± 0.7	150.5 ± 4	1.89 ± 0.06	3.10 ± 0.05	0.739	73.9	67.21
	9 × 10 $^{-6}$	109.10 ± 1	52.83 ± 0.5	127.9 ± 0.8	1.95 ± 0.03	3.20 ± 0.02	0.788	78.8	53.84
	11 × 10 $^{-6}$	108.40 ± 3	52.95 ± 0.4	139.5 ± 2	1.91 ± 0.02	3.08 ± 0.02	0.789	78.9	53.50

Corrosion current densities in the presence and absence of varied quantities of the examined chemicals are represented by the  $i_{\text{corr}}$  and  $i_{\text{corr}}^0$  symbols. The inhibition efficiency (%IE<sub>EFM</sub>) is affected by differences in individual approaches and different models utilized in interpretations [107, 108]. Utilizing EFM technology, a 10 mV potential signal disturbance amplitude was applied using two sine waves of 2 and 5 Hz. Three factors influence frequency selection [109]. The %IEEFM obtained from the testing is as follows: (1) > (2) > (3).

### 5.3 SEM Tests

In the absence and presence of  $1.1 \times 10^{-5}$  M perimidin-10-one derivatives (1–3), the miniature drawing obtained for the copper sample is shown in Fig. 15. When copper is submerged for three days and then placed in a blank, it suffers from severe destructive corrosion. The corrosion surface of copper not immersed in the solution is clearly different from the corroded one in the absence or presence of inhibitors, yet it appears to be reasonably consistent in roughness (pure sample). The polished trace left by emery sheets may be responsible for the narrow furrow seen in the uncorroded surface. As in the absence of inhibitors, the copper surface in 2 M HNO<sub>3</sub> appears uneven and pitted, whereas the surface immersed in the aggressive solution containing inhibitors became flat and tightly packed in compounds 1–3, implying that an

inhibitor adsorption layer formed on the surface and protected the metal from aggressive corrosion. The foregoing phenomenon revealed that the inhibitors investigated gave superior acid protection, which corresponded to corrosion inhibition results obtained using other methodologies [110, 111].

### 5.4 EDX Examination

It is used to determine the presence of elements on the surface of copper after being exposed to  $11 \times 10^{-6}$  M perimidin-10-one derivatives for 3 days in the absence of and presence of perimidin-10-one derivatives (1–3). Copper in an unfettered solution [Fig. 16 (pure sample), and Table 9] includes a higher percentage of copper, oxygen, and carbon atoms than copper in a 2MHNO<sub>3</sub>-dipped sample. When comparing the percentage exhibited in the blank spectrum to the spectrum of the sample in the presence of inhibitors [Fig. 16, Compounds (1–3)], it can be seen that the copper peaks are greatly reduced, indicating a reduction in the density of corrosion-active sites. Furthermore, the presence of inhibitors raised the peaks of oxygen and carbon, confirming the presence of our researched inhibitors on the copper surface [112]. All of these findings indicate that the corrosion of copper is reduced after inhibitor molecules are added. These findings are not surprising, given the presence of aromatic rings and heteroatoms, which enable the adsorption of the tested molecules to the copper surface, resulting in excellent corrosion resistance.

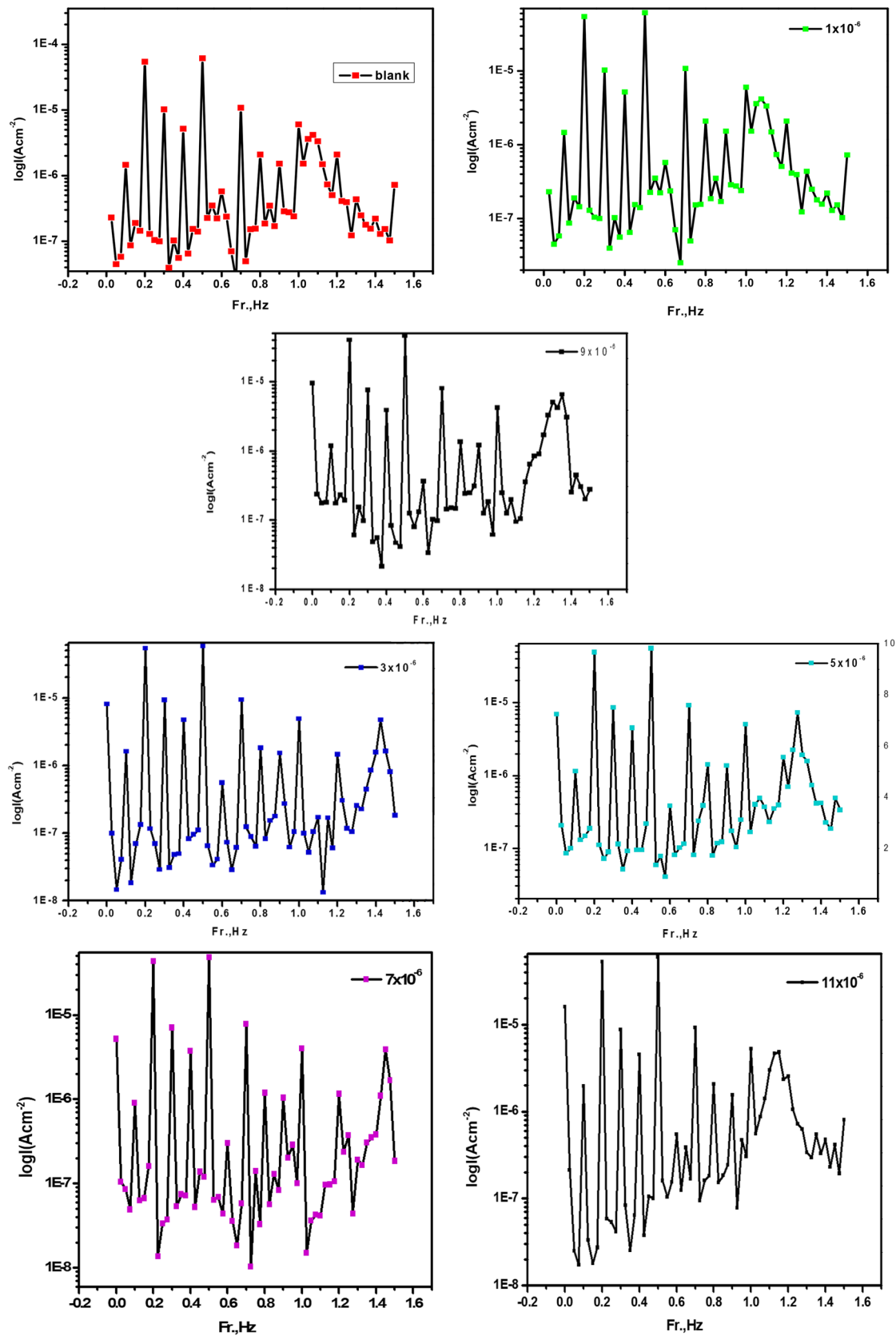


Fig. 14 EFM data for Cu nonexistence and existence-altered doses of composite (1) at  $30 \pm 1$  °C

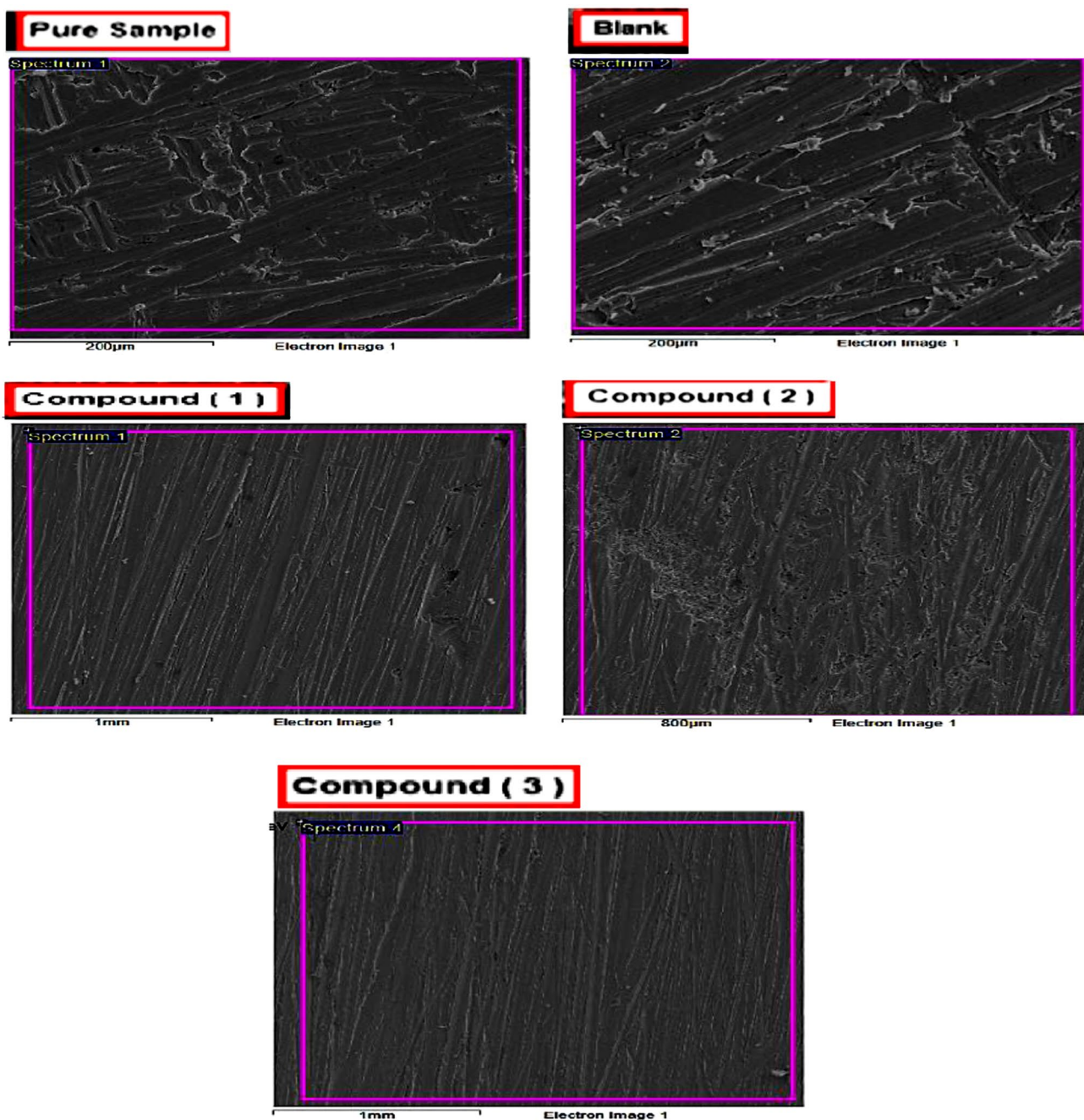


Fig. 15 SEM analysis of Cu after dipped in nonexistence and existence doses of  $11 \times 10^{-6}$  M

The results of the weight loss and electrochemical tests are supported by surface characterization analyses.

### 5.5 Quantum Theory

$E_{\text{HOMO}}$  levels reflect the ease with which electrons can be delivered to an acceptable receptor with unpackaged molecular orbitals. The ability of these molecules to receive electrons is determined by  $E_{\text{LUMO}}$  data. The higher the molecule's

capacity to receive electrons with lower  $E_{\text{LUMO}}$  values, but when the compound's  $E_{\text{HOMO}}$  values are high, the greater the compound's capability to provide electrons for those who are in the copper surface's unoccupied orbit ( $d$ -orbit), allowing for superior defense [113, 114]. Tables 10 and 11 show the quantum chemistry characteristics that are required for the experimental research of inhibitors in neutral and proton forms, namely  $E_{\text{LUMO}}$ ,  $E_{\text{HOMO}}$ , dipole moment ( $\mu$ ), energy  $E$  cavity, and molecule surface area. In two situations, Figs. 17,

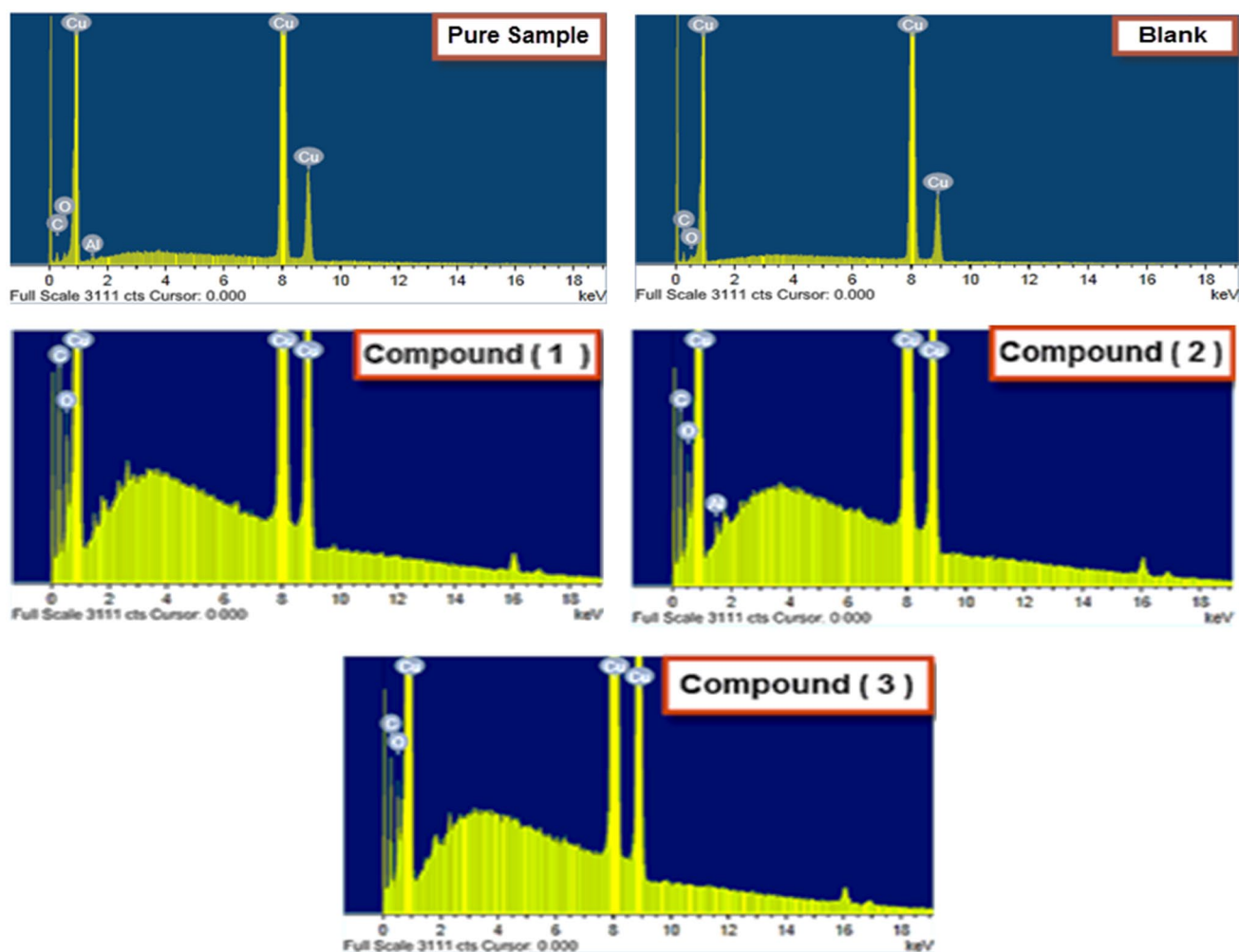


**Fig. 16** EDX test of Cu after dipped for days existence and nonexistence of  $11 \times 10^{-6}$  M of perimidin-10-one derivatives (1–3)

**Table 9** Mass % of Cu of plunged in acidic solution in an existence and nonexistence of  $11 \times 10^{-6}$  M of perimidin-10-one derivatives (1–3)

Elements (mass %)	C	O	Al	Cu
Pure sample	9.28	1.90	0.47	88.36
Blank	11.99	1.52	–	86.49
(1)	17.42	3.38	–	79.20
(2)	15.31	2.41	0.25	82.03
(3)	14.02	2.48	–	83.50

18, 19, and 20 show the best structure and shape for inhibitors (LUMO and HOMO orbitals) (neutral and protonated). Tables 10 and 11 show that compound (1) has the highest  $E_{\text{HOMO}}$  energy values, implying that it will provide the best corrosion protection. The energy gap ( $\Delta E$ ) is a crucial parameter that indicates the reaction of the inhibitor molecule via adsorption on the metal surface. The molecule's

response grows as the energy gap narrows. Because of the low ionization energy required to remove the electron from the orbital outer shell, a small value for the energy gap results in good corrosion inhibitors [115]. When comparing the neutral and proton forms of the inhibitors investigated, we discovered that the proton forms have a lower energy gap ( $\Delta E$ ) than the neutral form, implying that the inhibitors have a stronger reactivity toward the copper surface in the proton form. According to the previous information, soft particles have a small energy gap, are more polarized, and are frequently associated with high stability, giving better protection. The inhibitor (1) has the smallest energy gap, according to Table 10. This suggests that compound (1) has a higher contact with the other selected compounds and may easily adsorb on the copper surface, providing better corrosion protection, as evidenced by the probe data. The energy gap implies that the inhibitor efficiency arrangement is  $1^{\circ} 2^{\circ} 3^{\circ}$  and that experimental treatments produce the same arrangement. To explore and explain the structure, the dipole



**Table 10** The quantum measurements for investigated perimidin-10-one derivatives (1–3)

	Factors	Comp. (1)	Comp. (2)	Comp. (3)
PM3	$-E_{\text{HOMO}}$ (eV)	7.106	6.917	6.809
	$-E_{\text{LUMO}}$ (eV)	4.794	2.574	2.277
	$\Delta E$ (eV)	2.312	4.343	4.532
	$\eta$ (eV)	1.156	2.171	2.266
	$\sigma$ (eV) <sup>-1</sup>	0.865	0.460	0.441
	$-Pi$ (eV)	5.950	4.745	4.543
	$\chi$ (eV)	5.950	4.745	4.543
	Dipole moment (debyes)	8.475	7.266	6.815
	Molecular area (Å <sup>2</sup> )	398.846	388.477	373.084
	$\Delta N_{\text{max}}$ (e)	-0.635	-0.061	-0.0139
DMol3	$-E_{\text{HOMO}}$ (eV)	-4.439	-4.565	-4.349
	$-E_{\text{LUMO}}$ (eV)	-2.769	-2.871	-2.652
	$\Delta E$ (eV)	1.67	1.694	1.697
	$\eta$ (eV)	0.835	0.847	0.8485
	$\sigma$ (eV) <sup>-1</sup>	1.197	1.181	1.179
	$-Pi$ (e)	3.618	3.608	3.5005
	$\chi$ (eV)	3.618	3.608	3.5
	Dipole moment (debyes)	11.9791	9.1980	7.7524
	Molecular area (Å <sup>2</sup> )	382.27	364.88	383.47
	$\Delta N_{\text{max}}$ (e)	0.516	0.514	0.577

**Table 11** The quantum measurements for investigated perimidin-10-one derivatives (1–3) in the protonated form

	Factors	Comp.(1)	Comp.(2)	Comp. (3)
PM3	$-E_{\text{HOMO}}$ (eV)	4.881	4.995	4.79
	$-E_{\text{LUMO}}$ (eV)	4.771	4.776	4.65
	$\Delta E$ (eV)	0.11	0.219	0.14
	$\eta$ (eV)	0.055	0.1095	0.07
	$\sigma$ (eV) <sup>-1</sup>	18.18	9.13	14.28
	$-Pi$ (eV)	4.826	4.886	4.72
	$\chi$ (eV)	4.826	4.886	4.72
	Dipole moment (debyes)	10.476	10.794	11.998
	Molecular area (Å <sup>2</sup> )	3.94.44	372.474	388.722
	$\Delta N_{\text{max}}$ (e)	3.1	1.85	3.42
DMol3	$-E_{\text{HOMO}}$ (eV)	3.311	3.321	3.411
	$-E_{\text{LUMO}}$ (eV)	2.901	2.909	3.007
	$\Delta E$ (eV)	0.41	0.412	0.404
	$\eta$ (eV)	0.205	0.206	0.202
	$\sigma$ (eV) <sup>-1</sup>	4.87	4.85	4.95
	$-Pi$ (e)	3.106	3.115	3.21
	$\chi$ (eV)	3.106	3.115	3.21
	Dipole moment (debyes)	12.7622	10.33	11.022
	Molecular area (Å <sup>2</sup> )	387.13	366.39	384.46
	$\Delta N_{\text{max}}$ (e)	-3.35	-3.31	-3.14

moment is overused [116]. Because of the strong dipolar interactions between the copper surface and the selected compounds due to high values of  $\mu$ , adsorption on the copper surface becomes solid, resulting in a higher %IE [117]. A study of dipole moments reveals that the shape of the dipole moment in protons has changed dramatically, implying that proton-inhibiting particles are physically adsorbed onto the copper surface [118]. Absolute hardness  $\eta$  and softness  $\sigma$ , which are used to quantify the stability and response of molecules, are another essential property. Molecules with a big energy gap are more difficult to break than those with a small gap. Because they supply electrons to their recipients, soft particles are more reactive than hard ones. Adsorption may occur in a section of the inhibitor's molecule where the softness is at its maximum value [119] to get a small transfer of electrons. Derivative chemicals molecules form Lewis base in the corrosion group, but copper becomes Lewis acid. Bulk metals are more active with soft-base inhibitors. Table 10 shows the best relative agreement of  $Pi$  and  $\Delta N$  with inhibition efficacy and those connected to factors that improve  $Pi$  and  $\Delta N$  and will improve the inhibitor molecule's electronic release capability. The inhibitory effect caused by electron donation was shown by the  $N$  value [120–122]. When  $\Delta N < 3.6$ , both the power of donating electrons on the metal surface and the inhibition efficiency improve [123]. Two approaches were introduced, which leveraged a link between the molecule's molecular area and protection productivity. The efficiency of inhibition is increased by expanding the area of the molecules of the specified compounds; this is because the interaction area between the molecule and the surface of copper is increased.

## 5.6 Mulliken Charges and Fukui Indices

Knowing the donor and acceptor of the molecule's active centers is crucial, so we will use Mulliken atomic charges and Fukui indices to figure out where they are. The results of the various electrophilic and nucleophilic positions from neutral and protonated particles from compound 1, compound 2, and compound 3 are summarized in Table 12. Table 12 shows that the Mulliken distribution values are both negative and positive, indicating that the inhibitor compounds include active sites (donor–acceptor) that improve the sensitivity of these species to copper atoms. We noticed that the direction of all the values of the proton molecule positions grew dramatically, indicating an increase in the proton inhibitors' molecular interaction, and so this finding represents the neutral molecules' receptive nature. In terms of total negative charge (TNC), similar behavior was observed based on the results obtained in Table 12 and depicted in Fig. 21, with the TNC increasing after the inhibitor was protonated [124]. This indicates that the structural interaction of protonated particles is increasing. Compound

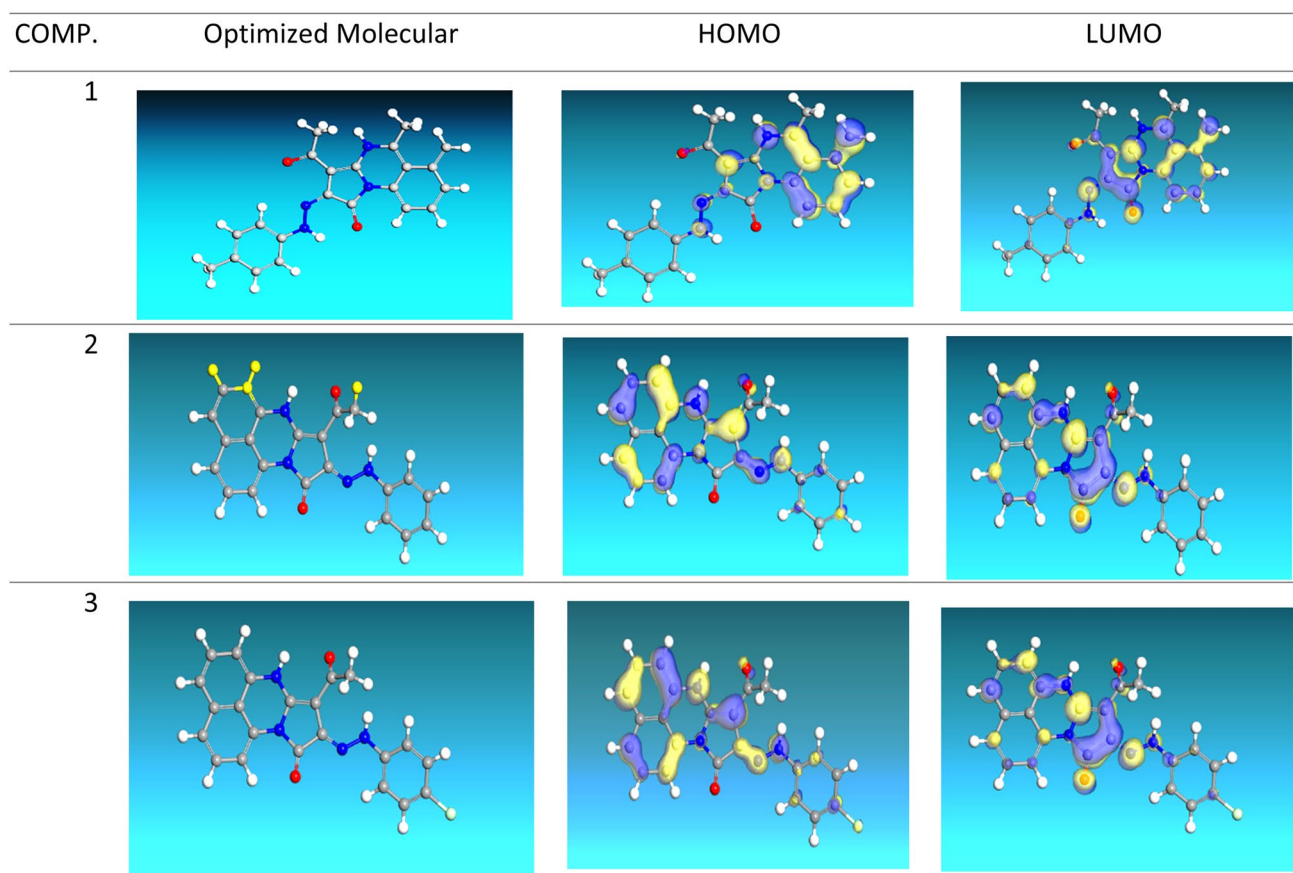


**Fig. 17** The molecular structures' optimization, HOMO, and LUMO for of investigated perimidin-10-one derivatives (1–3) using PM3 (neutral form)

1 has a stronger electron acceptor property than the other two compounds, according to TNC. Its capacity to be adsorbed onto the metal surface is improved as a result. These findings are consistent with those found in the investigative section organic compounds containing one or more heterocyclic atoms can develop at these locations in acid media ( $\text{HNO}_3$ ), resulting in positively charged particles. These interact with anions ( $\text{NO}_3^-$ ) that are widely spread on copper's surface. In this context, we will investigate this theory to determine the effect of the proton on the inhibitory molecules' local centers. As a result of this signal, the atoms of the studied molecules with higher values of  $f_k^+$  and  $f_k^-$  are depicted in proton and non-proton form in Fig. 22. The overall analysis of this picture reveals that each molecule has the identical atoms for both electrophilic and nucleophilic attack systems. The atom in the molecule with the highest Fukui function ( $f^+$ ), which is linked to the LUMO and degrades the reactivity to donor reagent, is the preferred site for nucleophilic assault. The atom in the molecule with the highest value of the Fukui function ( $f^-$ ) is chosen for electrophilic attack because it is related to the HOMO and gives the reactivity

toward an acceptor reagent. The atoms O(17) and N(18), C(16), and C(2) are favored sites for electrophilic attack, according to an analysis of the Fukui functions displayed in Fig. 22 because these sites have higher values of the Fukui function ( $f^-$ ) in the protonated form. The atoms C(2), C(16), and O(17) are the most vulnerable to nucleophilic assault because they have the greatest Fukui function ( $f^+$ ) values in the protonated state.

### 5.7 Molecular Electrostatic Potential (MESP)

The molecular electrostatic potential (MESP) has long been used to indicate the location of a chemical reaction. Electrostatic potential is colored differently at different spots on the electron density's surfaces. The electrically active and electrophilic zone is colored as red, and the majority of the electrostatic potential is negative. The color blue denotes the regions with the highest positive electrostatic potential (nucleophilic Region), whereas green denotes a region with no probability [125].

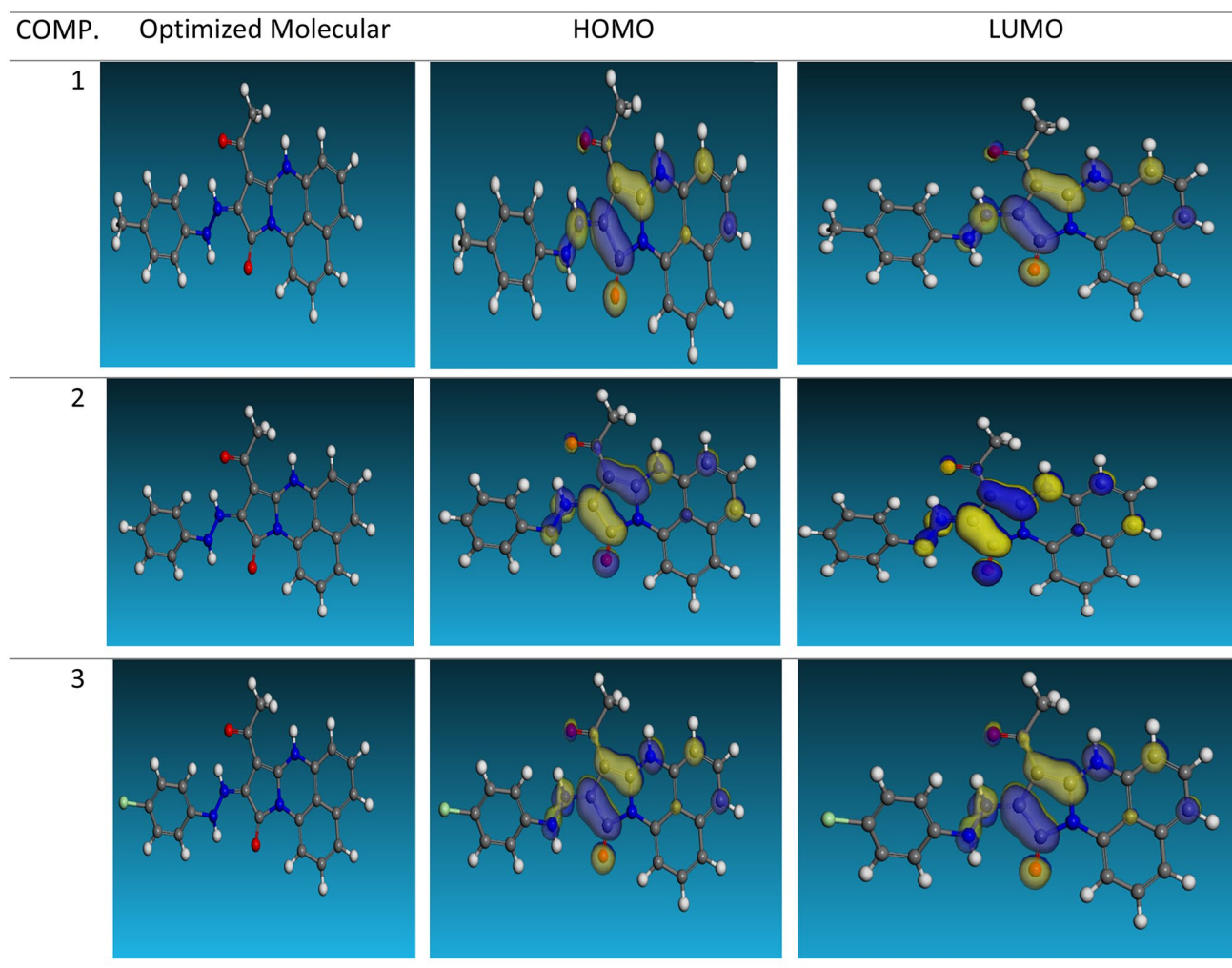


**Fig. 18** The molecular structures' optimization, HOMO, and LUMO for of investigated perimidin-10-one derivatives (1–3) using PM3 (protonated form)

The heteroatoms and double conjugate bonds are primarily located in electron-rich locations. Negative zones that prefer electrophilic assaults are indicated by oxygen, nitrogen, and chloride groups. Nucleophilic assaults are preferred by blue-colored hydrogen atoms (positive sign) (Fig. 23).

### 5.8 Simulation of Molecular Dynamics

In this research, we carefully selected the appropriate prearrangement for the uptake of inhibitor molecules on the Cu (1 1 1) substrate, which was completed by the adsorption locator shown in Fig. 24. Total energy, solid adsorption, and deformation energies are shown in Table 13 as the Monte Carlo simulation outputs. Calculation of total energy ( $\text{kcal mol}^{-1}$ ) for the production of the substrate—the adsorbent as a blend of solid adsorption energy energies of the molecules and deformation energy. Copper surface energy (1 1 1) was treated as zero in our research. Adsorption of energy

( $\text{kcal mol}^{-1}$ ) is the energy liberation that occurs when soothing chemicals are adsorbed for relaxation (the compounds examined are adsorbed on the surface of the substrate). The adsorbate molecules' adsorption energy is a mix of deformation and solid adsorption energy. Disturbed adsorption molecules are adsorbed on the substrate, and the constant adsorption energy ( $\text{kcal mol}^{-1}$ ) is released prior to the geometry optimization stage. Deformation energy ( $\text{kcal mol}^{-1}$ ) is the energy generated when adsorbed adsorbent components are positioned on the surface of the substrate [126].

Furthermore, the energy obtained is  $dE_{\text{ads}}/dN_i$  when one of the adsorbate molecules is removed from the adsorbent substrate formation ( $\text{kcal mol}^{-1}$ ). Table 12 shows the adsorption energies of the derivatives we looked at. Compound 1 is the most effective compound, according to the results in this table, because it has a higher adsorption capacity than the other compounds over the simulation period [127]. As a result, the molecules of compound 1 are very probably

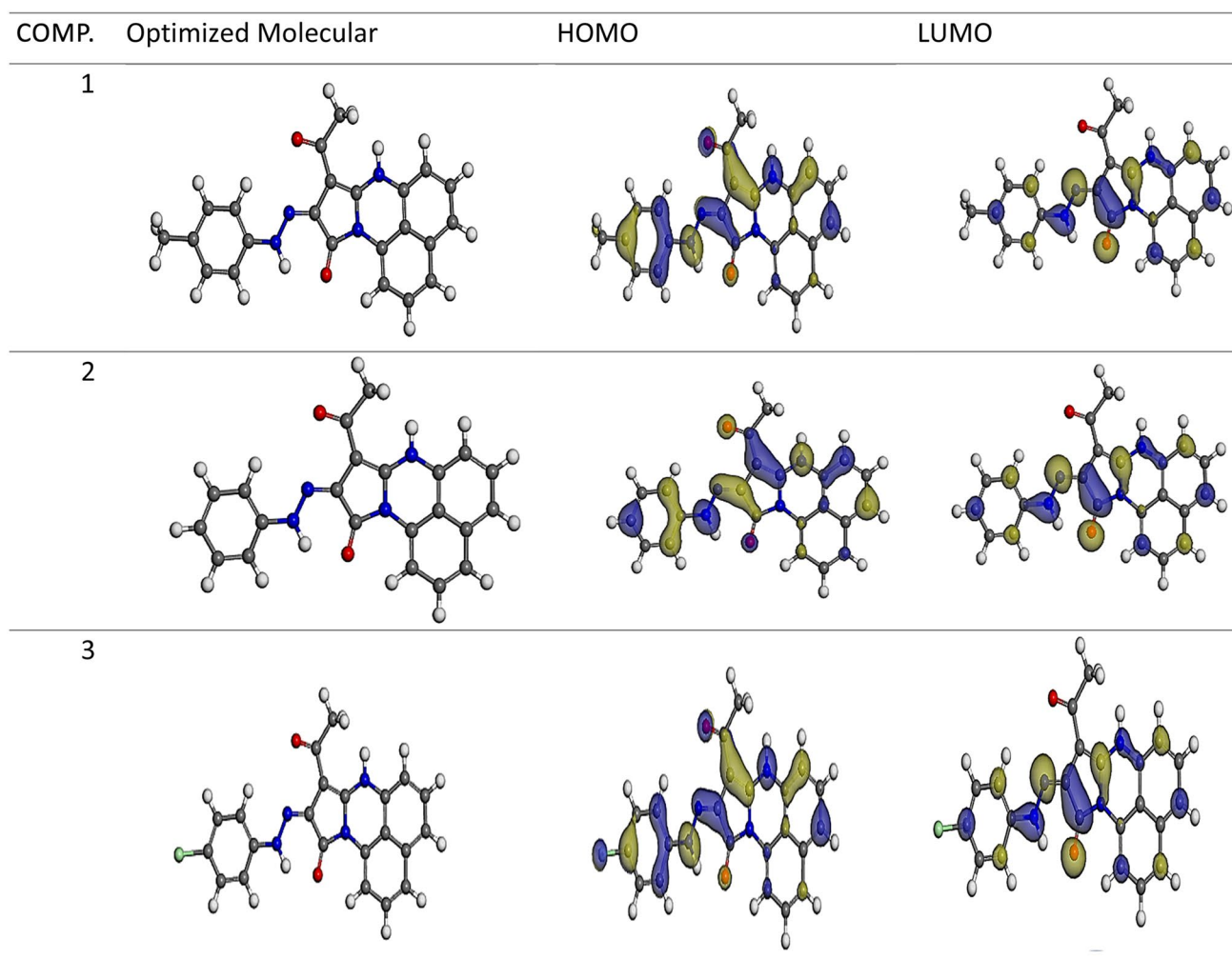


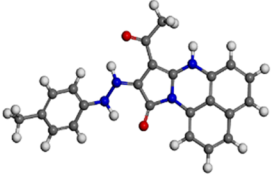
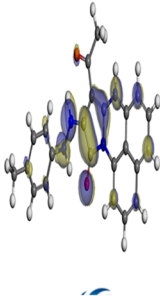
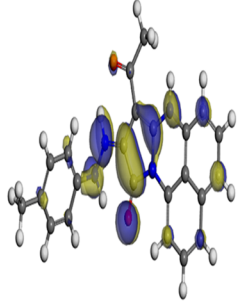
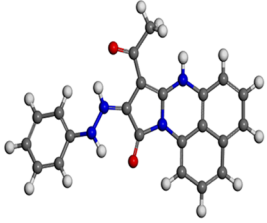
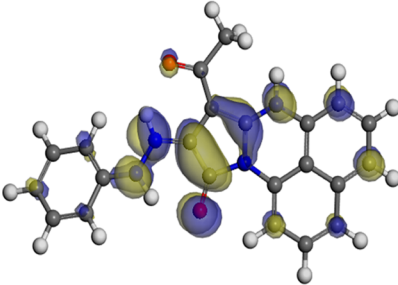
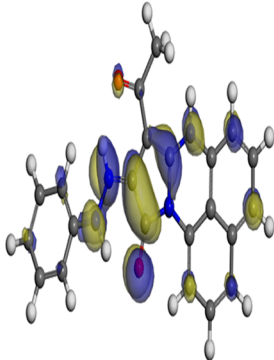
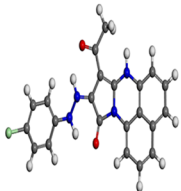
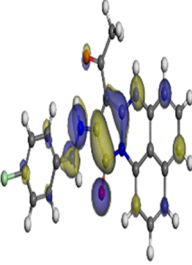
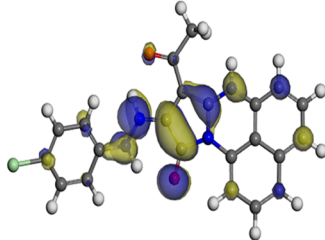
**Fig. 19** The molecular structures optimization, HOMO, and LUMO, for compounds (1–3) using DMol3/GGA/BOP (neutral form)

adsorbed on the surface of copper, forming more adsorbed layers of the other two compounds, giving protection against nitric acid corrosion on the copper surface, as demonstrated by theoretical and experimental research. The examined components offer outstanding results (high adsorption energy) in solution according to Tables 13 and 14 and previous studies [121, 128, 129]. Close examination indicates that the molecular structure of the local molecule is parallel to the surface. This adsorption pattern will be used by the components of the retarding particles to optimize the target metal's contact area or surface covering qualities (i.e., copper). The larger metal/inhibitor contact area will decrease substrate access instead of undesired nitrate anion assaults [130–133]. The adsorbent compounds could have a more flat shape. Their electrons or charges (which can be found in heterocyclic atoms, conjugate rings, and double bonds) are put into metallic sites (empty orbitals), establishing an inhibitory/metallic coordination bond [130–133]. The electron transfer is expected to be in reverse in the case of a

charged proton component, i.e., from the metallic surface to the inhibitor, causing the reversal of reaction. As a result, our inhibitor molecules adsorb confidently on the copper surface, generating strong adsorbent layers that protect the copper surface from nitric acid corrosion, as shown in both experimental and theoretical investigations (Table 14). We looked at molecule adsorption in both an acidic (neutral and proton) and a vacuum environment (Fig. 25). The adsorption energies climb above the vacuum value in the presence of an aqueous solution, suggesting that particle adsorption on the copper surface is more efficient (see Tables 13 and 15 for more information).

### 5.9 Chemical Structure of Corrosion Hindrance

Some perimidin-10-one derivatives (1–3) were tested for corrosion protection of copper in 2.0 M HNO<sub>3</sub> using ML, potentiodynamic polarization, EIS, and EFM tests, and it was discovered that the effectiveness of inhibition was

COMP.	Optimized Molecular	HOMO	LUMO
1			
2			
3			

**Fig. 20** The molecular structures optimization, HOMO, and LUMO, for compounds (1–3) using DMol3/GGA/BOP (protonated form)

dependent on the dose and nature of the metal, surface conditions, and inhibitor placement adsorption. The interaction of  $\pi$ -electrons from the compounds examined with the copper metal, the interaction of electron pairs not involved in the molecule, the electrostatic attraction between charged particles, and the integration of the above conditions [9] are all examples of adsorption that can be produced by inhibiting our compounds.  $\pi$ -electrons' centers as benzene rings and the existence of heterogeneous atoms are present in perimidin-10-one derivatives (oxygen and nitrogen). As a result, its presence on the surface of copper promotes the adsorption of molecules produced from Perimidin-10-one

derivatives [134]. The effect of these chemicals on corrosion value is detailed in the following: (1) A larger inhibitor dose reduced CR and  $i_{\text{corr}}$ . (2) ML allows for a linear shift in time. (3) Move potentiodynamic polarization to the greatest location feasible. (4) The number of active adsorption sites in a molecule and the density of its charge determine the %IE. In the aggressive medium, the rank of IE percent for Perimidin-10-one derivatives was as follows: (1) > (2) > (3). Copper corrosion in nitric acid ( $\text{HNO}_3$ ) is known to be autocatalytic, with nitrous acid ( $\text{HNO}_2$ ) as an intermediate product [135]. Because acid reduction results in a significant drop in free energy, the principal displacement of  $\text{H}^+$  ions

**Table 12** Changed values of Mulliken loads and Fukui indices of neutral and protonated inhibitory molecules

	Different values of Mulliken loads of neutral and protonated inhibitory molecules					
	Compound (1)		Compound (2)		Compound (3)	
	Neutral	Protonated	Neutral	Protonated	Neutral	Protonated
N (1)	- 0.478	- 0.471	- 0.479	- 0.472	- 0.472	- 0.473
C (2)	0.444	0.433	0.422	0.433	0.445	0.433
N (3)	- 0.393	- 0.394	- 0.412	- 0.393	- 0.391	- 0.39
C (4)	0.256	0.256	0.266	0.255	0.252	0.249
C (5)	- 0.115	- 0.12	- 0.113	- 0.119	- 0.117	- 0.122
C (6)	- 0.031	- 0.031	- 0.015	- 0.033	- 0.04	- 0.04
C (7)	- 0.082	0.086	- 0.068	- 0.084	- 0.084	- 0.089
C (8)	0.078	0.08	0.098	0.079	0.068	0.067
C (9)	- 0.074	- 0.082	- 0.065	- 0.081	- 0.077	- 0.084
C (10)	- 0.029	- 0.031	- 0.016	- 0.031	- 0.04	- 0.04
C (11)	- 0.112	- 0.117	- 0.101	- 0.119	- 0.112	- 0.118
C (12)	0.263	0.261	0.265	0.263	0.257	0.255
C (13)	0.009	0.008	0.009	0.008	0.003	0
C (14)	- 0.025	- 0.014	- 0.018	- 0.014	- 0.032	- 0.022
C (15)	0.102	0.157	0.107	0.16	0.098	0.151
C (16)	0.459	0.424	0.458	0.421	0.462	0.421
O (17)	- 0.553	- 0.607	- 0.529	- 0.604	- 0.55	- 0.599
N (18)	- 0.23	- 0.265	- 0.199	- 0.265	- 0.239	- 0.27
N (19)	- 0.201	- 0.291	- 0.201	- 0.287	- 0.203	- 0.282
C (20)	0.261	0.259	0.282	0.265	0.262	0.256
C (21)	- 0.089	- 0.091	- 0.076	- 0.089	- 0.08	- 0.083
C (22)	- 0.057	- 0.055	- 0.008	- 0.024	- 0.055	- 0.054
C (23)	0.057	0.053	- 0.03	- 0.056	0.035	0.033
C (24)	- 0.052	- 0.054	- 0.004	- 0.022	- 0.05	- 0.054
C (25)	- 0.101	- 0.109	- 0.083	- 0.107	- 0.095	- 0.105
C (26)	- 0.1	- 0.098	0.293	0.31	- 0.103	- 0.109
C (27)	0.29	0.307	- 0.442	- 0.573	0.286	0.306
O (28)	- 0.543	- 0.572	- 0.172	- 0.182	- 0.537	- 0.567
C (29)	- 0.183	- 0.181	0.166	0.21	- 0.209	- 0.207
H (30)	0.209	0.211	0.008	0.045	0.216	0.218
H (31)	0.047	0.045	0.015	0.039	0.058	0.055
H (32)	0.041	0.039	0.008	0.03	0.051	0.049
H (33)	0.033	0.03	0.008	0.031	0.044	0.041
H (34)	0.034	0.031	0.017	0.038	0.045	0.042
H (35)	0.04	0.038	0.071	0.06	0.051	0.048
H (36)	0.063	0.06	0.197	0.226	0.077	0.072
H (37)	0.2	0.226	0.013	0.21	0.215	0.238
H (38)	0.038	0.207	0.008	0.035	0.06	0.221
H (39)	0.028	0.034	0.006	0.031	0.054	0.056
H (40)	0.025	0.025	0.011	0.027	0.052	0.052
H (41)	0.051	0.024	0.064	0.03	0.064	0.051
H (42)	0.032	0.037	0.041	0.038	0.079	0.059
H (43)	0.045	0.035	0.041	0.075	0.083	0.084
H (44)	0.041	0.044	0.059	0.075	0.065	0.085
H (45)	0.074	0.034		0.059		0.069
H (46)	0.069	0.074				
H (47)	0.053	0.076				
H (48)		0.058				

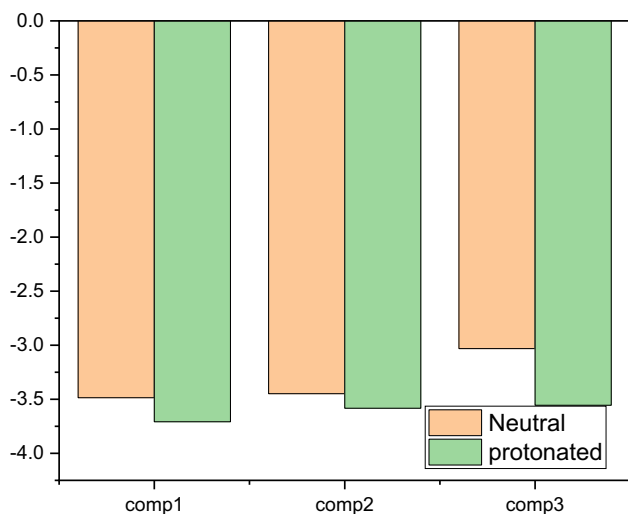
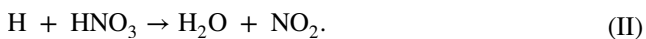
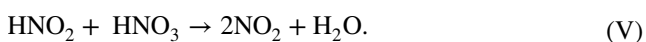


**Fig. 21** TNC of three inhibitors protonated and nonprotonated molecules

from solution is followed by  $\text{HNO}_3$  reduction rather than hydrogen evolution:

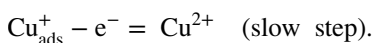
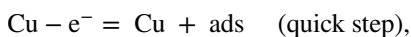


Each nitrous dioxide ( $\text{NO}_2$ ) molecule forms and performs the chain propagation mechanism below, yielding two  $\text{NO}_2$  [136] molecules. It has been reported [137] that inhibitors compounds capable of interacting with  $\text{HNO}_2$  produced in this manner can slow down the rate of copper dissolution in acid:



The suppression found after adding the inhibitors [138, 139] has been attributed to their destruction of  $\text{HNO}_2$  generated as described in Eq. (IV), which would block the autocatalytic growth.

The dissolution of copper in nitric acid is accomplished in two steps [131]:



$\text{Cu}^+$  ions are adsorbed to the first equation on the copper surface during these processes, and these ions do not diffuse

in the common solution [140]. The dissolving stage of copper is controlled by the propagation of soluble  $\text{Cu}^{++}$  ions from the outer Helmholtz plane to the bulk solution. The inhibitor molecules are easily protonated in  $\text{HNO}_3$  solution, resulting in positively charged inhibitor species. In light of this, it was necessary to compute the surface charge of copper at zero, also known as the zero charge potential (ZCP). The value of  $(E_{\text{corr}} - E_{\text{q}} = 0)$  can be used to compute it. The surface charge is positive when the value  $(E_{\text{corr}} - E_{\text{q}} = 0)$  is greater than zero [141]. In  $\text{HNO}_3$  solution, the ZCP of copper is  $E_{\text{q}} = -40$  mV vs. SCE as determined elsewhere [142]. Returning to Table 6, the maximum  $E_{\text{corr}}$  values for compounds **1**, **2**, and **3** in 2 M  $\text{HNO}_3$  are  $-34.6$ ,  $26.8$ , and  $26.8$  mV vs. SCE measured at  $11 \times 10^{-6}$  M, respectively. As a result, the computed values of Cu-ZCP are  $5.4$ ,  $13.2$ , and  $13.2$  mV, respectively, indicating that the copper surface is positively charged.

The charged copper surface attracts nitrate ions. The results were based on the assumption that nitrate ions can cling to a positively charged surface. The number of nitrate ions, neutral forms of perimidin-10-one derivatives (**1–3**), and their proton derivatives in bulk solution can be significantly higher. These proton forms form an electrical link between the investigated molecule and the copper surface's negative charge [143–145]. Another mechanism relies on partial electron transmutation from oxygen and nitrogen atoms, coordination bonds, and non-positional  $\pi$  electrons in the perimidin-10-one derivatives (**1–3**) rings being generated by  $\text{Cu}^{2+}$  ion-free d orbitals at the copper surface. Furthermore, both physical and chemical adsorption can occur throughout the adsorption process. Because the oxide layer that protects the copper surface from corrosion does not form [85, 86]. The breakdown of copper into  $\text{Cu}^{2+}$  [121] and the action of a clutch of  $\text{Cu}^{2+}$  ions at the copper surface are the basis for this process. These conditions are mitigated by the formation of d empty orbitals with low energy in copper, as seen in transition metal metals. Perimidin-10-one derivative (**1**) has the highest %IE due to: I the presence of the p-CH<sub>3</sub> group, which is a donating electron group with a  $-ve$  Hammett constant ( $\sigma = -0.17$ ); additionally, p-CH<sub>3</sub> will improve the density of electron charge on the molecule, and (ii) its larger molecular size, which allows it to be more easily adsorbed on the Cu surface. In terms of %IE, perimidin-10-one derivatives (**2**) come in second. Because of its smaller molecular size and the absence of a substituent in the p-position (H-atom with a value of  $\sigma = 0.0$ ). Perimidin-10-one derivatives (**3**) have the lowest %IE due to the presence of p-Cl, which has  $+ve$   $\sigma_{\text{Cl}} = +0.23$ , implying that the p-Cl group reduces the electron density on the molecule and hence, lesser %IE.

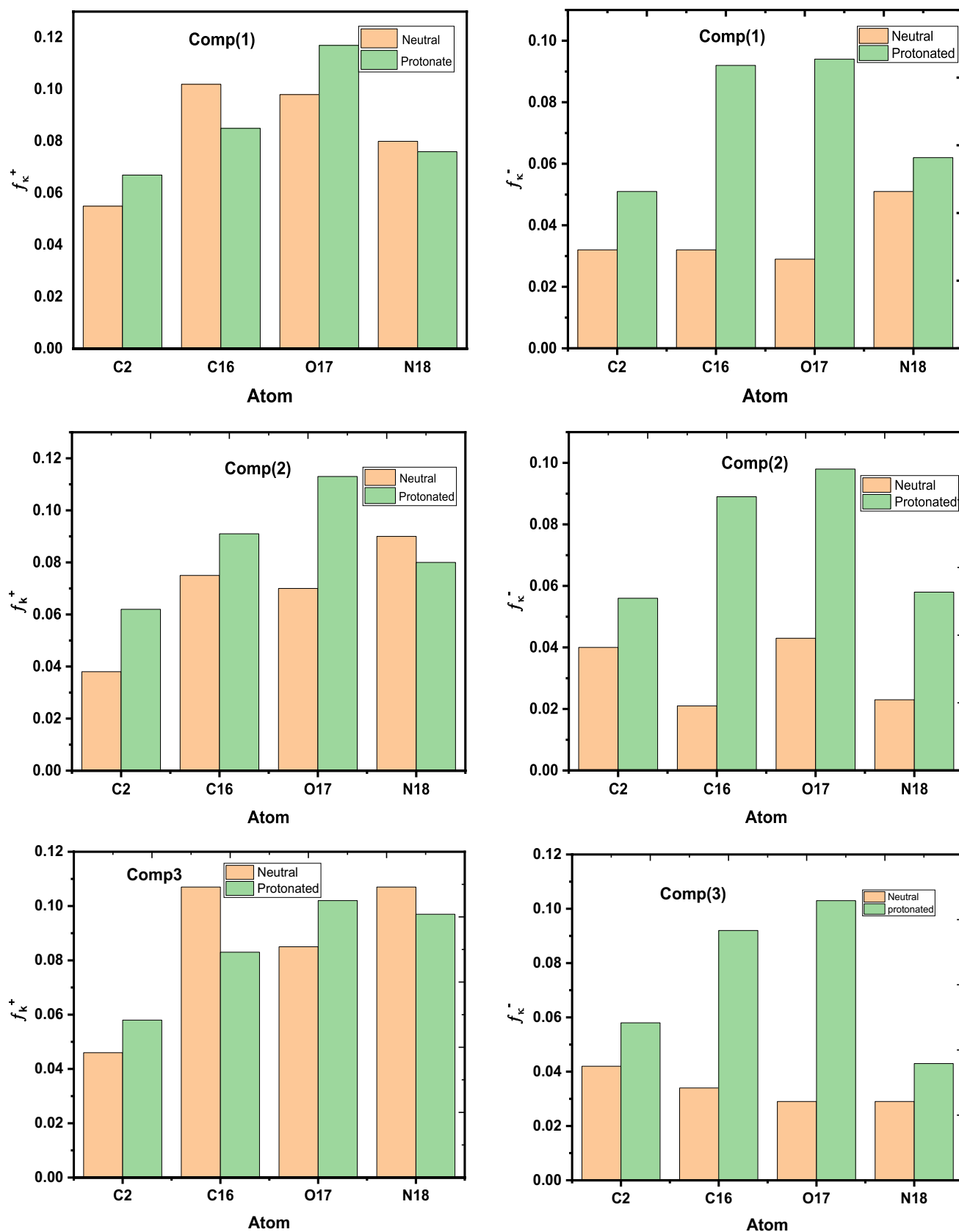
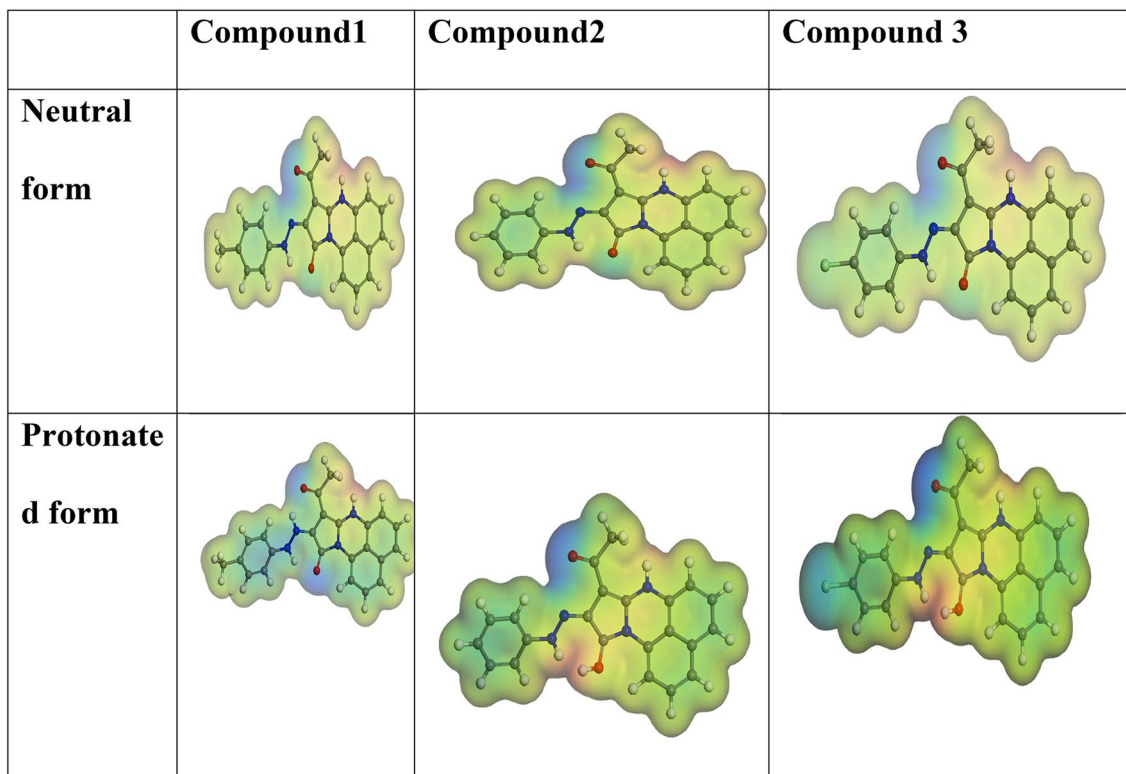


Fig. 22 Graphical representation of the Fukui indices of inhibitors for the more reactive atoms in the un-protonated and protonated form





**Fig. 23** Pictures of the protonated and un-protonated molecular electrostatic potential with the electrostatic contour of the inhibitor

## 6 Conclusion

The perimidin-10-one derivatives (**1–3**) inhibit Cu corrosion in 2.0 M HNO<sub>3</sub> and follow the Florry–Huggins isotherm for adsorption, where this isotherm indicate to physical adsorption for these compounds. Chemical and electrochemical measurements show that the inhibitory efficiency increases as the concentrations of our studied compounds increase, whereas the inhibitory efficiency decreases as the temperature rises. Furthermore, double-layer capacitances decrease as the concentrations of the

chemicals we studied rise. The molecules' adsorption on the copper surface is aided by this property. In 2.0 M HNO<sub>3</sub>, the used inhibitors behave as a mixed-kind inhibitor, according to potentiodynamic polarization data. The morphology of shielded and unprotected Cu has been studied using SEM and EDX. The findings of the investigation and theoretical analysis supported the hypothesis that compounds (**1**, **2** and **3**) are effective corrosion inhibitors and that the following factors influence the efficacy of inhibition of perimidin-10-one derivatives: (**1**) > (**2**) > (**3**).

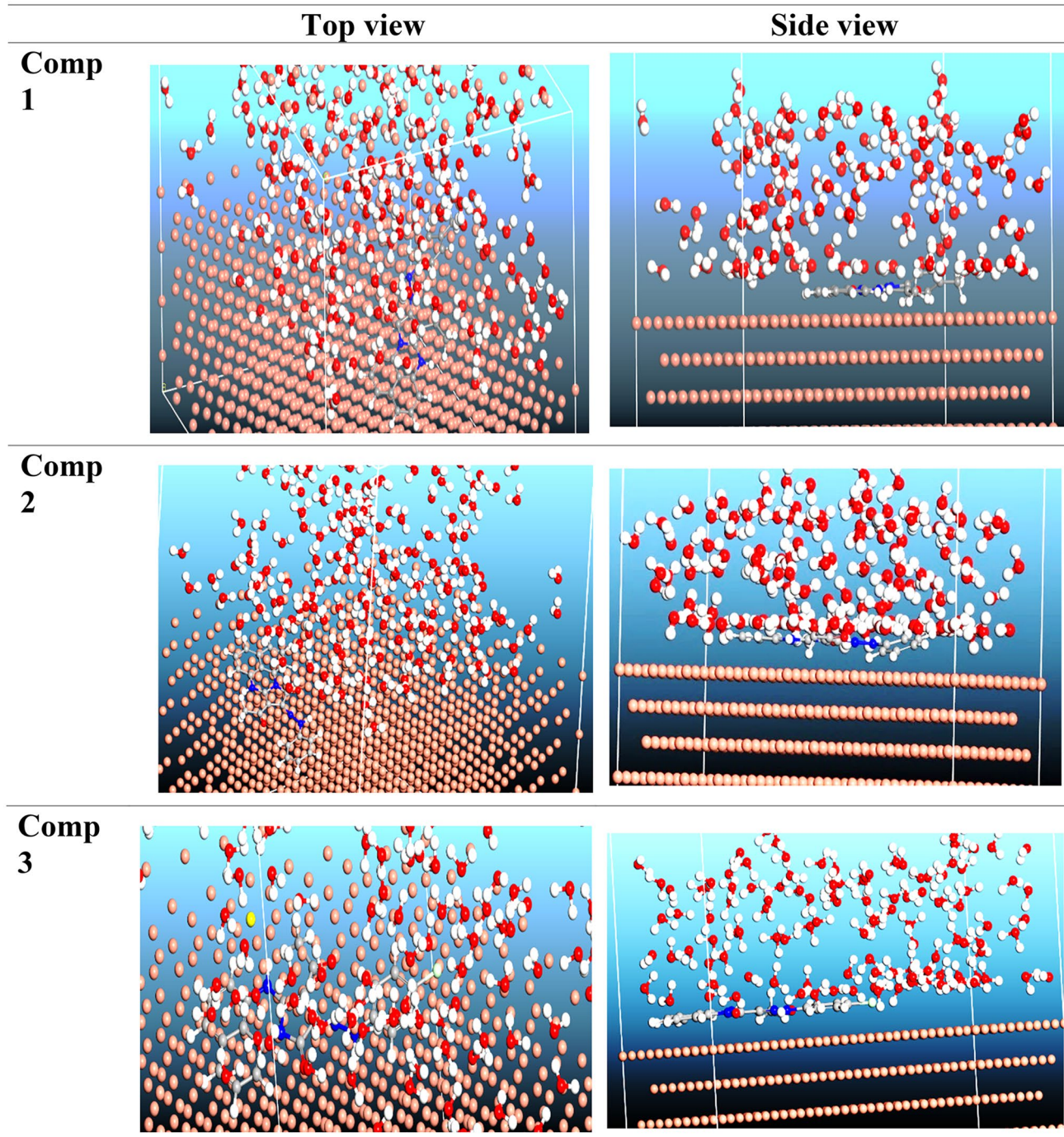


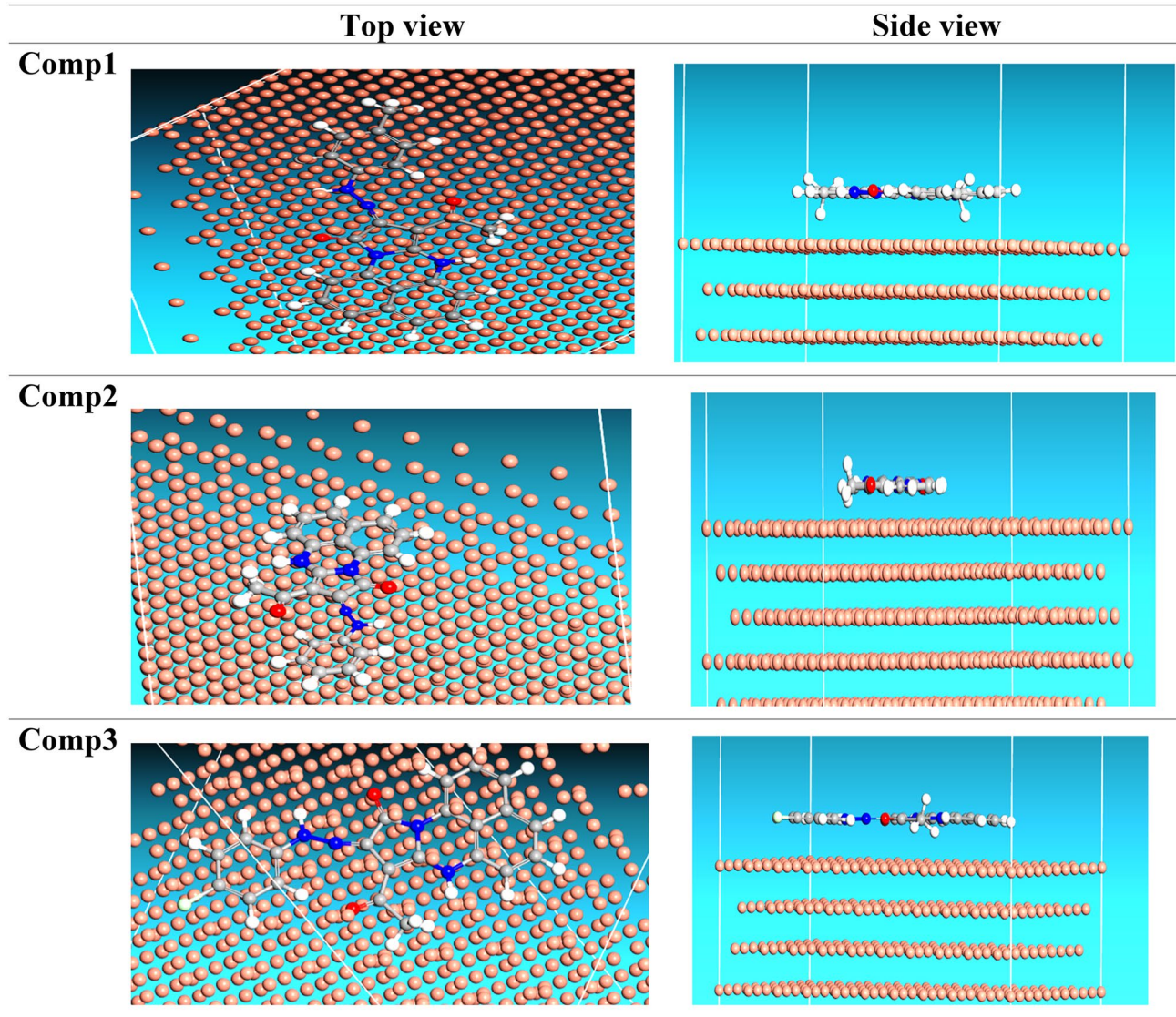
**Fig. 24** The most suitable formation for adsorption of Perimidin-10-one derivatives molecules (1–3) on Cu (1 1 1) substrate got by adsorption locator module (neutral form)

**Table 13** Data and descriptions calculated by Monte Carlo simulation for the inhibitor adsorption on copper (1 1 1)

Structures Cu (1 1 1)	Total energy $k$ (cal mol <sup>-1</sup> )	Adsorption energy $k$ (cal mol <sup>-1</sup> )	Rigid adsorption energy $k$ (cal mol <sup>-1</sup> )	Deformation energy $k$ (cal mol <sup>-1</sup> )	$dE_{\text{ads}}/dN_i$ $k$ (cal mol <sup>-1</sup> )
Compound 1	- 2888.7	- 2822.2	- 2981.8	160.07	- 139.3
Compound 2	- 2858.3	- 2797.3	- 2957.1	159.3	- 132.0
Compound 3	- 2802.1	- 2728.2	- 2882.1	- 153.6.6	- 113.6

**Table 14** Data and descriptions calculated by Monte Carlo simulation for the inhibitor adsorption (protonated form) on copper (1 1 1)

Structures Cu (1 1 1)	Total energy $k$ (cal mol <sup>-1</sup> )	Adsorption energy $k$ (cal mol <sup>-1</sup> )	Rigid adsorption energy $k$ (cal mol <sup>-1</sup> )	Deformation energy $k$ (cal mol <sup>-1</sup> )	$dE_{\text{ads}}/dN_i$ $k$ (cal mol <sup>-1</sup> )
Compound 1	- 2868.3	- 2831.8	- 2987.3	156.14	- 144.40
Compound 2	- 2871.6	- 2799.6	- 2959.9	160.37	- 144.38
Compound 3	- 2866.5	- 2792.4	- 2952.5	160.12	- 134.52

**Fig. 25** The most suitable form for adsorption of Perimidin-10-one derivatives molecules (1–3) on Cu (1 1 1) substrate obtained by adsorption locator module without aqueous solution

**Table 15** Data and descriptions intended by simulating Monte Carlo for uptake of inhibitors on copper (111) in a vacuum

Structures Cu (111)	Total energy $k$ (cal mol <sup>-1</sup> )	Adsorption energy $k$ (cal mol <sup>-1</sup> )	Rigid adsorption energy $k$ (cal mol <sup>-1</sup> )	Deformation energy $k$ (cal mol <sup>-1</sup> )	$dE_{\text{ads}}/dN_i$ $k$ (cal mol <sup>-1</sup> )
Compound 1	- 188.3	- 567.2	- 118.60	- 448.6	- 567.3
Compound 2	- 181.3	- 112.8	- 117.75	- 4.92	- 112.8
Compound 3	- 173.9	- 109.9	- 112.79	2.84	- 109.9

**Supplementary Information** The online version contains supplementary material available at <https://doi.org/10.1007/s40735-022-00650-8>.

**Funding** There were no research Grants for this work from any funding agencies.

**Data Availability** All data generated or analyzed during this study are included in this published article.

## Declarations

**Conflict of interest** The authors declare that they have no known competing financial interests or personal relationships that could have appeared to influence the work reported in this paper.

## References

- Toumiat K, Guibadj A, Taouti MB (2017) Copper corrosion inhibition using btah inhibitor in sodium chloride medium: experimental and theoretical studies. *Eurasian J Anal Chem* 12(3):275–294. <https://doi.org/10.12973/ejac.2017.00170a>
- Satpati AK, Reddy AVR (2011) Electrochemical study on corrosion inhibition of copper in hydrochloric acid medium and the rotating ring-disc voltammetry for studying the dissolution. *Int J Electrochem* 2011:173462–1734609. <https://doi.org/10.4061/2011/173462>
- Rahal HT, Abdel-Gaber AM, Younes GO (2016) Inhibition of steel corrosion in nitric acid by sulfur containing compounds. *Chem Eng Commun* 203:435–445. <https://doi.org/10.1080/00986445.2015.1017636>
- Karthik G, Sundaravadivelu M, Rajkumar P, Manikandan M (2015) Diaza-adamantane derivatives as corrosion inhibitor for copper in nitric acid medium. *Res Chem Intermed* 41:7593–7615. <https://doi.org/10.1007/s11164-014-1846-8>
- Tansuğ G, Tüken T, Giray ES, Fındıkkıran G, Sığırcık G, Demirkol O, Erbil M (2014) A new corrosion inhibitor for copper protection. *Corr Sci* 84:21. <https://doi.org/10.1016/j.corsci.2014.03.004>
- Feroz-Khan P, Shanthi V, Babu RK, Muralidharan S, ChandraB-anik R (2015) Effect of benzotriazole on corrosion inhibition of copper under flow conditions. *J Environ Chem Eng* 3(1):10–19. <https://doi.org/10.1016/j.jece.2014.11.005>
- Vrsalović L, Gudić S, Gracić D, Smoljko I, Ivanić I, Kliškić M, Oguzie EE (2018) Corrosion protection of copper in sodium chloride solution using Propolis. *Int J Electrochem Sci* 13:2102–2117. <https://doi.org/10.20964/2018.02.71>
- Udochukwu Ofoegbu S, Galvão TLP, Gomes JRB, Tedim J, Nogueira HIS, Ferreira MGS, Zheludkevichac ML (2017) Corrosion inhibition of copper in aqueous chloride solution by 1H-1,2,3-triazole and 1,2,4-triazole and their combinations: electrochemical, Raman and theoretical studies. *Phys Chem Chem Phys* 19:6113–6129. <https://doi.org/10.1039/c7cp00241f>
- Feng L, Zhang S, Qiang Y, Xu Y, Guo L, Madkour LH, Chen S (2018) Experimental and theoretical investigation of thiazolyl blue as a corrosion inhibitor for copper in neutral sodium chloride solution. *Materials* 11:1042–1059. <https://doi.org/10.3390/ma11061042>
- Arshad N, Rehman Akram A, Akram M, Rasheed I (2017) Triazolothiadiazine derivatives as corrosion inhibitors for copper, mild steel and aluminum surfaces: electrochemical and quantum investigations. *Prot Met Phys Chem Surf* 53(2):343–358. <https://doi.org/10.1134/S2070205117020046>
- Fouda AEAS, Etaiw SH, El-Azziz DMA, Elbaz OA (2017) Synergistic effect of barium chloride on corrosion inhibition of copper by aqueous extract of lupine seeds in nitric acid. *Int J Electrochem Sci* 12:5934–5950. <https://doi.org/10.0964/2017.07.08>
- Fouda AS, Fouad RR (2016) New azonitrile derivatives as corrosion inhibitors for copper in nitric acid solution, *Cogent. Chemistry* 2:1221174–1221188. <https://doi.org/10.1080/23312009.2016.1221174>
- Zarrouk, Hammouti B, Zarrok H, Bouachrine M, Khaled KF, Al-Deyab SS (2012) Corrosion inhibition of copper in nitric acid solutions using a new triazole derivative. *Int J Electrochem Sci* 7:89–105
- Khaled KF, Amin MA (2009) Dry and wet lab studies for some benzotriazole derivatives as possible corrosion inhibitors for copper in 1.0 M HNO<sub>3</sub>. *Corros Sci* 51:2098–2106
- Fouda AS, El-Dossoki FI, Shady IA (2018) Adsorption and corrosion inhibition behavior of polyethylene glycol on α-brass alloy in nitric acid solution. *Green Chem Lett Rev* 11:67–77. <https://doi.org/10.1080/17518253.2018.1438525>
- Fiala A, Chibani A, Darchen A, Boukamh A, Djebbar K (2007) Investigations of the inhibition of copper corrosion in nitric acid solutions by ketene dithioacetal derivatives. *Appl Surf Sci* 253:9347–9356. <https://doi.org/10.1016/j.apsusc.2007.05.066>
- Howida A, Fetouh M (2014) Tarek and Abdel-Fattah, Novel plant extracts as green corrosion inhibitors for 7075–T6 aluminium alloy in an aqueous medium. *Int J Electrochem Sci* 9:1565–1582
- Abiola OK, James AO (2010) The effects of *Aloe vera* extract on corrosion and kinetics of corrosion process of zinc in HCl solution. *Corros Sci* 52:661–664. <https://doi.org/10.1016/j.corsci.2009.10.026>
- Eldesoky AM, Hassan HM, Fouda AS (2013) Studies on the corrosion inhibition of copper in nitric acid solution using some pharmaceutical compounds. *Int J Electrochem Sci* 8:10376–10395
- Fouda AS, Wahid HA (2016) Corrosion inhibition of copper in HNO<sub>3</sub> solution using thiophene and its derivatives. *Arab J Chem* 9:S91–S99. <https://doi.org/10.1016/j.arabjc.2011.02.014>
- Arrousse N, Salima R, Kaddouri Y, Zarrouk A, Zahri D, El Hajjaji F, Touzani R, Taleb M, Jodehd S (2020) The inhibition behavior of two pyrimidine-pyrazole derivatives

- against corrosion in hydrochloric solution: experimental, surface analysis and in silico approach studies. *Arab J Chem* 13(7):5949–5965
22. Echihi S, Benzbiria N, Belghiti ME, El Fal M, Boudalia M, Essassi EM, Guenbour A, Bellaouchou A, Tabyaoui M, Azzi M (2021) Corrosion inhibition of copper by pyrazole pyrimidine derivative in synthetic seawater: experimental and theoretical studies. *Mater Today Proc* 37(3):3958–3966
  23. Xu Y, Zhang S, Guo L, Tan B, Liao C, Zhou Y, Madkour LH (2018) Halogen-substituted pyrazolo-pyrimidine derivatives as corrosion inhibitors for copper in sulfuric acid solution. *Int J Corros Scale Inhib* 7(2):236–249
  24. Xu S, Zhang S, Guo L, Feng L, Tan B (2019) Experimental and theoretical studies on the corrosion inhibition of carbon steel by two indazole derivatives in HCl medium. *Materials* 12:1339–1349. <https://doi.org/10.3390/ma12081339>
  25. Khaled KF (2010) Corrosion control of copper in nitric acid solutions using some amino acids—a combined experimental and theoretical study. *Corros Sci* 52:3225–3234. <https://doi.org/10.1016/j.corsci.2010.05.039>
  26. Scendo M, Uznanska J (2011) The effect of ionic liquids on the corrosion inhibition of copper in acidic chloride solutions. *Int J Corros* 2011:718626–718638. <https://doi.org/10.1155/2011/718626>
  27. Sherif EM, Park S-M (2006) Effects of 2-amino-5-ethylthio-1,3,4-thiadiazole on copper corrosion as a corrosion inhibitor in aerated acidic pickling solutions. *Electrochim Acta* 51:6556–6562. <https://doi.org/10.1016/j.electacta.2006.04.047>
  28. Ignat I, Varvara S, Muresan L (2015) *Studia Universitatis Babeş-Bolyai, Chemia*, 60(LX):127
  29. Wei N, Jiang Y, Liu Z, Ying Y, Guo X, Wu Y, Wen Y, Yang H (2018) 4-Phenylpyrimidine monolayer protection of a copper surface from salt corrosion. *RSC Adv* 8:7340–7349. <https://doi.org/10.1039/C7RA12256J>
  30. Farahatia R, Ghaffarinejad A, Morteza Mousavi-Khoshdel S, Rezanian J, Behzadi H, Shockraavid A (2019) Synthesis and potential applications of some thiazoles as corrosion inhibitor of copper in 1 M HCl: experimental and theoretical studies. *Prog Org Coat* 132:417–428. <https://doi.org/10.1016/j.porgcoat.2019.04.005>
  31. Rhattas K, Benmessaoud M, Doubi M, Hajjaji N, Srhiri A (2011) Corrosion inhibition of copper in 3% NaCl solution by derivative of aminotriazole. *Mater Sci Appl* 2(4):220–225. <https://doi.org/10.4236/msa.2011.24028>
  32. Fouda AS, Eldesoky AM, Diab MA, Nabih A (2016) Inhibitive, adsorption studies on carbon steel corrosion in acidic solutions by new synthesized benzene sulfonamide derivatives. *Int J Electrochem Sci* 11:9998–10019. <https://doi.org/10.20964/2016.12.47>
  33. Sherif EM, Shamy AM, Ramla MM, ElNashawy AOH (2007) 5-(Phenyl)-4H-1,2,4-triazole-3-thiol as a corrosion inhibitor for copper in 3.5% NaCl solutions. *J Mater Chem Phys* 102:231–239. <https://doi.org/10.1016/j.matchemphys.2006.12.009>
  34. Valek L, Martinez S (2007) Copper corrosion inhibition by *Azadirachta indica* leaves extract in 0.5 M sulphuric acid. *Mater Lett* 61:148–151. <https://doi.org/10.1016/j.matlet.2006.04.024>
  35. Farghaly TA, Mahmoud HK (2013) Synthesis, tautomeric structures, and antitumor activity of new perimidines. *J Arch Pharm Chem Life Sci* 346:392–402. <https://doi.org/10.1002/ardp.201200486>
  36. ASTM (2004) AST G 31–72, Standard recommended practice for the laboratory immersion corrosion testing of metals. American Society for Testing and Materials, Philadelphia
  37. Zhou L, Lv Y-L, Hu Y-X, Zhao J-H, Xia X, Li X (2018) Experimental and theoretical investigations of 1,3,5-tris(4-aminophenoxy)benzene as an effective corrosion inhibitor for mild steel in 1 M HCl. *J Mol Liq* 249:179–187. <https://doi.org/10.1016/j.molliq.2017.10.129>
  38. Abd El-Lateef HM, Abo-Riya MA, Tantawy AH (2016) Empirical and quantum chemical studies on the corrosion inhibition performance of some novel synthesized cationic Gemini surfactants on carbon steel pipelines in acid pickling processes. *Corros Sci* 108:94–110. <https://doi.org/10.1016/j.corsci.2016.03.004>
  39. Pearson RG (1988) Absolute electronegativity and hardness application to inorganic chemistry. *Inorg Chem* 27:734–740
  40. Zhang Z, Huang X, Tian N, Ni F, Ruan L, Lv Y, Wu L (2016) Corrosion inhibition effect of histidine and its derivatives self-assembled films formed of 304 stainless steel. *Int J Electrochem Sci* 11:9175–9191. <https://doi.org/10.20964/2016.11.73>
  41. Fouda AS, Elewady GY, Shalabi K, Abdel-Aziz HK (2015) Alcamines as corrosion inhibitors for reinforced steel and their effect on cement based materials and mortar performance. *RSC Adv* 5:36957–36968. <https://doi.org/10.1039/c5ra00717h>
  42. Gong Z, Peng Sh, Huang X, Gao L (2018) Investigation the corrosion inhibition effect of itraconazole on copper in H<sub>2</sub>SO<sub>4</sub> at different temperatures: combining experimental and theoretical studies. *Materials* 11:2107–2123. <https://doi.org/10.3390/ma1112107>
  43. Kumar A, Trivedi M, Sharma RK, Singh G (2017) Synthetic, spectral and structural studies of a Schiff base and its anticorrosive activity on mild steel in H<sub>2</sub>SO<sub>4</sub>. *New J Chem* 41:8459–8468. <https://doi.org/10.1039/c7nj00896a>
  44. Fragoza-Mar L, Olivares-Xometl O, Domínguez-Aguilar MA, Flores EA, Arellanes-Lozada P, Jiménez-Cruz F (2012) Corrosion inhibitor activity of 1,3-diketone malonates for mild steel in aqueous hydrochloric acid solution. *Corros Sci* 61:171–184. <https://doi.org/10.1016/j.corsci.2012.04.031>
  45. Harckerman N, Hurd RM (1962) 1st International congress on metallic corrosion, vol 166. Butterworths, London
  46. Lgaz H, Salghi R, Jodeh S, Hammouti B (2017) Effect of clozapine on inhibition of mild steel corrosion in 1.0 M HCl medium. *J Mol Liq* 225:271–280. <https://doi.org/10.1016/j.molliq.2016.11.039>
  47. Aoun SB (2017) On the corrosion inhibition of carbon steel in 1 M HCl with a pyridinium ionic liquid: chemical, thermodynamic, kinetic and electrochemical studies. *RSC Adv* 7:36688–36696. <https://doi.org/10.1039/c7ra04084a>
  48. Amin A, Khaled KF, Mohsen Q, Arida A (2010) A study of the inhibition of iron corrosion in HCl solutions by some amino acids. *Corros Sci* 52:1684–1695. <https://doi.org/10.1016/j.corsci.2010.01.019>
  49. Umoren SA, Ogbobe O, Igwe IO, Ebenso EE (2008) Inhibition of mild steel corrosion in acidic medium using synthetic and naturally occurring polymers and synergistic halide additives. *Corros Sci* 50:1998–2006. <https://doi.org/10.1016/j.corsci.2008.04.015>
  50. Keera S, Deyab M (2005) Effect of some organic surfactants on the electrochemical behaviour of carbon steel in formation water. *Colloids Surf A* 266:129–140. <https://doi.org/10.1016/j.colsurfa.2005.05.069>
  51. Hassan AM, Abdel-Fatah TMH (2016) Aqueous extract of *Salvadora persica* as a novel green corrosion inhibitor for low-alloy steel in acidic media—Part I. *Int J Electrochem Sci* 11:6959–6975. <https://doi.org/10.20964/2016.08.48>
  52. Abd El Rehim S, Hassan H, Amin M (2003) The corrosion inhibition study of sodium dodecyl benzene sulphonate to aluminium and its alloys in 1.0 M HCl solution. *Mater Chem Phys* 78:337–348. [https://doi.org/10.1016/S0254-0584\(01\)00602-2](https://doi.org/10.1016/S0254-0584(01)00602-2)

53. Hammouti B, Dafali A, Touzani R, Bouachrine M (2012) Inhibition of copper corrosion by bipyrazole compound in aerated 3% NaCl. Saudi Chem Soc 16:413–418. <https://doi.org/10.1016/j.jscs.2011.02.009>
54. Mu G, Li X, Liu G (2005) Synergistic inhibition between tween 60 and NaCl on the corrosion of cold rolled steel in 0.5 M sulfuric acid. Corros Sci 47:1932–1952. <https://doi.org/10.1016/j.corsci.2004.09.020>
55. Putilova J, Balezin S, Bacannik IN, Bishop VP (1960) Metal corrosion inhibitors. Pergamon, Oxford, p 1196
56. Bourazmi H, Tabyaoui M, El Hattabi L, El Aoufir Y, Ebenso EE, Ansari A (2018) Camphor as an effective corrosion inhibitor for carbon steel in 1 M HCl solution: electrochemical and quantum chemical investigation. J Mater Environ Sci 9(3):1058–1074. <https://doi.org/10.26872/jmes.2017.9.3.118>
57. El Faydy M, Touir R, Ebn Touhami M, Zarrouk A, Jama C, Lakhrissi B, Olasunkanmi LO, Ebenso EE, Bentiss F (2018) Corrosion inhibition performance of newly synthesized 5-alkoxy-methyl-8-hydroxyquinoline derivatives for carbon steel in 1 M HCl solution: experimental, DFT and Monte Carlo simulation studies. Phys Chem Chem Phys 20:20167–20187. <https://doi.org/10.1039/c8cp03226b>
58. Motawea MS, Abdelaziz MA (2015) Some pyrazole derivatives as corrosion inhibitors for carbon steel in hydrochloric acid solutions. Eur J Chem 6(3):342–349. <https://doi.org/10.5155/eurjchem.6.3.342-349.1279>
59. Savita, Mourya P, Chaubey N, Kumar S, Singh VK, Singh MM (2016) *Strychnos nuxvomica*, *Piper longum* and *Mucuna pruriens* seed extracts as eco-friendly corrosion inhibitors for copper in nitric acid. RSC Adv 6:95644–95655. <https://doi.org/10.1039/c6ra16481a>
60. Zarrouk A, Hammouti B, Dafali A, Bentiss F (2013) Inhibitive properties and adsorption of purpald as a corrosion inhibitor for copper in nitric acid medium. Ind Eng Chem Res 52:2560–2568. <https://doi.org/10.1021/ie301465k>
61. Zheng X, Gong M, Li Q, Guo L (2018) Corrosion inhibition of mild steel in sulfuric acid solution by loquat (*Eriobotrya japonica* Lindl.) leaves extract. Sci Rep 8:9140. <https://doi.org/10.1038/s41598-018-27257-9>
62. Gadow HS, Motawea MM (2017) Investigation of the corrosion inhibition of carbon steel in hydrochloric acid solution by using ginger roots extract. RSC Adv 7:24576–24588. <https://doi.org/10.1039/c6ra28636d>
63. Oukhrib R, El Issamia, El Ibrahim B, El Mouadena K, Bazzi L, Bammou L, Chaouay A, Salghi R, Jodeh S, Hammouti B, Amin-Alami A (2017) *Ziziphus lotus* as green inhibitor of copper corrosion in natural sea water. Portugaliae Electrochim Acta 35(4):187–200. <https://doi.org/10.4152/pea.201704187>
64. Talati JD, Modi RM (1986) Inhibition of corrosion of aluminum–copper alloy in NaOH. Trans SAEST 11:295
65. Thomas JM, Thomas WJ (1981) Introduction to the principles of heterogeneous catalysis, 5th edn. Academic Press, London, p 14
66. Putilova IN, Balezin SA, Barannik VP (1960) Metallic corrosion inhibitors. Pergamon Press, New York, p 31
67. Riggs OL Jr, Hurd RM (1967) Temperature coefficient of corrosion inhibition. Corrosion 23:252–260
68. Martinez S, Stern I (2001) Inhibitory mechanism of low-carbon steel corrosion by mimosa tannin in sulphuric acid solution. J Appl Electrochem 31:973–978
69. Abd El-Rehim SS, Ibrahim MAM, Khalid KF (2001) The inhibition of 4-(2'-amino-5'-methylphenylazo) antipyrine on corrosion of mild steel in HCl solution. Mater Chem Phys 70:268–273
70. Li X, Mu G (2005) Tween-40 as corrosion inhibitor for cold rolled steel in sulphuric acid: weight loss study, electrochemical characterization, and AFM. Appl Surf Sci 252:1254–1265
71. Tang L, Mu G, Liu G (2003) The effect of neutral red on the corrosion inhibition of cold rolled steel in 1.0 M hydrochloric acid. Corros Sci 45:2251–2262
72. Li X, Tang L (2005) Synergistic inhibition between OP and NaCl on the corrosion of cold-rolled steel in phosphoric acid. Mater Chem Phys 90:286–297
73. Laidler KJ (1963) Reaction kinetics, vol 1, 1st edn. Pergamon Press, New York
74. Zhang QB, Hua YX (2009) Corrosion inhibition of mild steel by alkyl imidazolium ionic liquids in hydrochloric acid. Electrochim Acta 54:1881–1887. <https://doi.org/10.1016/j.electacta.2008.10.025>
75. Krid F, Zouaoui E, Salah M (2018) Aqueous extracts of *Opuntia ficus-indica* as a green corrosion inhibitor of A283C carbon steel in sulfuric acid solution. Chem. Chem. Technol. 12(3):405–409. <https://doi.org/10.23939/chcht12.03.405>
76. Kamal C, Sethuraman MG (2012) Caulerpin—a bis-Indole alkaloid as a green inhibitor for the corrosion of mild steel in 1 M HCl solution from the marine alga *Caulerpa racemose*. Ind Eng Chem Res 51:10399–10407. <https://doi.org/10.1021/ie3010379>
77. Amin MA, Ahmed MA, Arida HA, Kandemirli F, Saracoglu M, Arslan T, Basaran MA (2011) Monitoring corrosion and corrosion control of iron in HCl by non-ionic surfactants of the TRITON-X series—Part III. Immersion time effects and theoretical studies. Corros Sci 53:1895–1909. <https://doi.org/10.1016/j.corsci.2011.02.007>
78. Moretti G, Guidi F, Fabris F (2013) Corrosion inhibition of the mild steel in 0.5 M HCl by 2-butyl-hexahydropyrrolo[1,2-b][1,2]oxazole. Corros Sci 76:206–218. <https://doi.org/10.1016/j.corsci.2013.06.044H>
79. Hamani H, Douadi T, Daoud D, Al-Noaimi M, Rikkouh RA, Chafaa S (2017) 1-(4-Nitrophenyl-imino)-1-(phenylhydrazono)-propane-2-one as a corrosion inhibitor for mild steel in 1 M HCl solution: Weight loss, electrochemical, thermodynamic and quantum chemical studies. J Electroanal Chem 801:425–438. <https://doi.org/10.1016/j.jelechem.2017.08.031>
80. Laamari MR, Benzakour J, Berrekhis F, Abouelfida A, Derja A, Villemin D (2016) Adsorption and corrosion inhibition of carbon steel in hydrochloric acid medium by hexamethylenediamine tetra (methylene phosphonic acid). Arab J Chem 9:S245–S251. <https://doi.org/10.1016/j.arabjc.2011.03.018>
81. Eldesoky AM, Diab MA, El-Sonbati AZ, Salam SF (2017) Anticorrosive properties of new eco-friendly dimethylamino compounds on C-steel corrosion in 2 M HCl. Int J Electrochem Sci 12:4215–4237. <https://doi.org/10.20964/2017.05.73>
82. Sing HA, Ebenso EE, Quraishi MA (2012) Stem extract of brahmi (*Bacopa monnieri*) as green corrosion inhibitor for aluminum in NaOH solution. Int J Electrochem Sci 7:3409–3419
83. Bothi Raja P, Sethuraman MG (2008) Atropine sulphate as corrosion inhibitor for mild steel in sulphuric acid medium. Mater Lett 62:1602–1604. <https://doi.org/10.1016/j.matlet.2007.09.032>
84. Pourbaix M (1975) Atlas of electrochemical equilibria in aqueous solutions. NACE, Houston
85. Johnson HE, Leja J (1965) On the potential/pH diagrams of the Cu–NH–H<sub>2</sub>O and Zn–NH–H<sub>2</sub>O systems. J Electrochem Soc 112:638–641. <https://doi.org/10.1149/1.2423629>
86. Fouda AS, Badawya AA (2019) Adsorption and corrosion inhibition of Cu in nitric acid by expired simvastatin drug. Prot Met Phys Chem Surf 55:572–582. <https://doi.org/10.1134/S2070205119030146>
87. Yan Y, Li W, Cai L, Hou B (2008) Electrochemical and quantum chemical study of purines as corrosion inhibitors for mild steel in 1 M HCl solution. Electrochim Acta 53:5953–5960. <https://doi.org/10.1016/j.electacta.2008.03.065>
88. Chen J, Qiang Y, Peng S, Gong Z, Zhang S, Gao L, Tan B, Chen S, Guo L (2018) Experimental and computational investigations

- of 2-amino-6-bromobenzothiazole as a corrosion inhibitor for copper in sulfuric acid. *J Adhes Sci Technol* 32(19):2083–2098. <https://doi.org/10.1080/01694243.2018.1460948>
89. Macdonald DD, Mckubre MCH (1982) Impedance measurements in electrochemical systems. In: Bockris JOM, Conway BE, White RE (eds) *Modern aspects of electrochemistry*, vol 14. Plenum Press, New York, p 61
  90. Ali SM, Al Lehaibi HA (2016) Control of zinc corrosion in acidic media: green fenugreek inhibitor. *Trans Nonferrous Met Soc China* 26:3034–3045. [https://doi.org/10.1016/S10036326\(16\)64434-5](https://doi.org/10.1016/S10036326(16)64434-5)
  91. Galai M, Benqlilou H, Ebn Touhami M, Belhaj T, Berrami K, ElKafssaoui H (2018) Comparative analysis for the corrosion susceptibility of copper alloys in sandy soil. *Environ. Eng. Res.* 23(2):164–174. <https://doi.org/10.4491/eer.2017.077>
  92. Outirite M, Lagrenee M, Lebrini M, Traisnel M, Jama C, Vezin H, Bentiss F (2010) Ac impedance, X-ray photoelectron spectroscopy and density functional theory studies of 3,5-bis(*n*-pyridyl)-1,2,4-oxadiazoles as efficient corrosion inhibitors for carbon steel surface in hydrochloric acid solution. *Electrochim Acta* 55:1670–1681. <https://doi.org/10.1016/j.electacta.2009.10.048>
  93. Muthukrishnan P, Prakash P, Jeyaprabha B, Shankar K (2015) Stigmasterol extracted from *Ficus hispida* leaves as a green inhibitor for the mild steel corrosion in 1 M HCl solution. *Arab J Chem.* <https://doi.org/10.1016/j.arabjc.2015.09.005>
  94. Mo S, Qin TT, Luo HQ, Li NB (2015) Insights into the corrosion inhibition of copper in hydrochloric acid solution by self-assembled films of 4-octylphenol. *RSC Adv* 5:90542–90549. <https://doi.org/10.1039/C5RA13074C>
  95. Chen W, Hong S, Xiang B, Luo H, Li M, Li N (2013) Corrosion inhibition of copper in hydrochloric acid by coverage with trithiocyanuric acid self-assembled, monolayers. *Corros Eng Sci Technol* 48(2):98–107. <https://doi.org/10.1179/1743278212Y.0000000053>
  96. Jwad Habeeb H, Mohammed Luaibi H, Mohammed Dakhil R, Abdul Amir Kadhum H, Ahmed Al-Amiery A, Sumer Gaaz T (2018) Development of new corrosion inhibitor tested on mild steel supported by the electrochemical study. *Results Phys* 8:1260–1267. <https://doi.org/10.1016/j.rinp.2018.02.015>
  97. Preethi Kumari P, Shetty P, Rao SA (2017) Electrochemical measurements for the corrosion inhibition of mild steel in 1 M hydrochloric acid by using an aromatic hydrazide derivative. *Arab J Chem* 10:653–663. <https://doi.org/10.1016/j.arabjc.2014.09.005>
  98. Kong P, Feng H, Chen N, Lu Y, Li S, Wang P (2019) Polyaniline/chitosan as a corrosion inhibitor for mild steel in acidic medium. *RSC Adv* 9:9211–9217. <https://doi.org/10.1039/c9ra00029a>
  99. Volpi E, Fioiadelli C, Trasatti S, Koleva D (2017) Development of smart corrosion inhibitors for reinforced concrete structures exposed to a microbial environment. *Ind Eng Chem Res* 56(20):5778–5794. <https://doi.org/10.1021/acs.iecr.7b00127>
  100. Ali IH, Suleiman MHA (2018) Effect of acid extract of leaves of *Juniperus procera* on corrosion inhibition of carbon steel in HCl solutions. *Int J Electrochem Sci* 13:3910–3922. <https://doi.org/10.20964/2018.04.01>
  101. Idusuyi N, Ajide OO, Oluwole OO, Arotiba OA (2017) Electrochemical impedance study of an Al6063–12%SiC–Cr composite immersed in 3 wt.% sodium chloride. *Procedia Manuf* 7:413–419
  102. Mohan R, Joseph A (2018) Corrosion protection of mild steel in hydrochloric acid up to 313 K using propyl benzimidazole electroanalytical, adsorption and quantum chemical studies. *Egypt J Pet* 27(1):11–20. <https://doi.org/10.1016/j.ejpe.2016.12.003>
  103. Benabdellah M, Tounsi A, Khaled KF, Hammouti B (2011) Thermodynamic, chemical and electrochemical investigations of 2-mercaptop benzimidazole as a corrosion inhibitor for mild steel in hydrochloric acid solutions. *Arab J Chem* 4:17–24. <https://doi.org/10.1016/j.arabjc.2010.06.010>
  104. Guo W, Chen S, Serb HMA (2006) A study of the inhibition of copper corrosion by triethyl phosphate and triphenyl phosphate self-assembled monolayers. *Serb Chem Soc* 71(2):167–175. <https://doi.org/10.2298/JSC0602167G>
  105. Amin MA, Mersal GAM, Mohsen Q (2011) Monitoring corrosion and corrosion control of low alloy ASTM A213 grade T22 boiler steel in HCl solutions. *Arab J Chem* 4(2):223–229. <https://doi.org/10.1016/j.arabjc.2010.06.040>
  106. Shalabi K, Abdallah YM, Fouda AS (2015) Corrosion inhibition of aluminum in 0.5 M HCl solutions containing phenyl sulfonylacetophenoneazo derivatives. *Res Chem Intermed* 41:4687–4711. <https://doi.org/10.1007/s11164-014-1561-5>
  107. Fouda AS, Nazeer AA, Saber A (2014) Electrochemical adsorption properties and inhibition of zinc corrosion by two chromones in sulfuric acid solutions. *J Korean Chem Soc* 58:160–168. <https://doi.org/10.5012/jkcs.2014.58.2>
  108. El-Haddad MN (2016) Inhibitive action and adsorption behavior of cefotaxime drug at copper/hydrochloric acid interface: electrochemical, surface and quantum chemical studies. *RSC Adv* 6:57844–57853. <https://doi.org/10.1039/c6ra03316d>
  109. El-Haddad MN, Fouda AS (2013) Corrosion inhibition and adsorption behavior of some azo dye derivatives on carbon steel in acidic medium : synergistic effect of halide ions. *Chem Eng Commun* 200:1366–1393. <https://doi.org/10.1080/00986445.2012.746675>
  110. Bosch RW, Bogaerts WF, Syrett B (2003) Proceedings of 8th international symposium on electrochemical methods in corrosion research modulation (EFM) technique, Nieuwpoort, Belgium, 4–9 May 2003
  111. Motawea MM, El-Hossiany A, Fouda AS (2019) Corrosion control of copper in nitric acid solution using *Chenopodium* extract. *Int J Electrochem Sci* 14:1372–1387. <https://doi.org/10.20964/2019.02.29>
  112. Mara Cortez Alves de Oliveira V, Aguiara C, Muci Vazqueza A, Laurent Marie Robin A, Justino Ribeiro Barboza M (2017) Corrosion behavior analysis of plasma-assisted PVD coated Ti–6Al–4V alloy in 2 M NaOH solution. *Mater Res* 20:436–404
  113. Prabhu R, Venkatesha T, Shanbhag A, Kulkarni G, Kalkhambkar R (2008) Inhibition effects of some Schiff's bases on the corrosion of mild steel in hydrochloric acid solution. *Corros Sci* 50:3356–3362. <https://doi.org/10.1016/j.corsci.2008.09.009>
  114. Idouhli R, N'Ait Outside A, Koumya Y, Abouelfida A, Benayach A, Auhmani A, Itto MYA (2018) Electrochemical studies of monoterpene thiosemicarbazones as corrosion inhibitor for steel in 1 M HCl. *Int J Corros* 2018:9212705–9212719. <https://doi.org/10.1155/2018/9212705>
  115. Lopez DA, Simison SN, de Sanchez SR (2005) Inhibitors performance in CO<sub>2</sub> corrosion EIS studies on the interaction between their molecular structure and steel microstructure. *Corros Sci* 47:735–755. <https://doi.org/10.1016/j.corsci.2004.07.010>
  116. Satapathy AK, Gunasekaran G, Sahoo Kumar SC, Rodrigues APV (2009) Corrosion inhibition by *Justicia gendarussa* plant extract in hydrochloric acid solution. *Corros Sci* 51:2848–2856. <https://doi.org/10.1016/j.corsci.2009.08.016>
  117. Ebenso EE, Arslan T, Kandemirli F, Caner N, Love I (2010) Quantum chemical studies of some rhodanine azosulpha drugs as corrosion inhibitors for mild steel in acidic medium. *Int J Quant Chem* 110:1003–1018. <https://doi.org/10.1002/qua.22249>
  118. Ozcan M, Dehri I, Erbil M (2004) Organic sulfur-containing compounds as corrosion inhibitors for mild steel in acidic media: correlation between inhibition efficiency and chemical structure. *Appl Surf Sci* 236:155–164. <https://doi.org/10.1016/j.apsusc.2004.04.017>

119. Ansari KR, Ramkumar S, Nalini D, Quraishi MA (2016) Studies on adsorption and corrosion inhibitive properties of quinoline derivatives on N80 steel in 15% hydrochloric acid. *Cogent Chem* 2:1145032–1145045. <https://doi.org/10.1080/23312009.2016.1145032>
120. Mert BD, Mert ME, Kardas ME, Yazici G (2011) Experimental and theoretical investigation of 3-amino-1,2,4-triazole-5-thiol as a corrosion inhibitor for carbon steel in HCl medium. *Corros Sci* 53:4265–4272. <https://doi.org/10.1016/j.corsci.2011.08.038>
121. Roque JM, Pandiyan T, Cruz J, Garcí'a-Ochoa E (2008) DFT and electrochemical studies of tris(benzimidazole-2-ylmethyl)amine as an effective corrosion inhibitor for carbon steel surface. *Corros Sci* 50:614–624. <https://doi.org/10.1016/j.corsci.2007.11.012>
122. Gece G (2008) The use of quantum chemical methods in corrosion inhibitor studies. *Corros Sci* 50:2981. <https://doi.org/10.1016/j.corsci.2008.08.043>
123. Musa AY, Kadhum AH, Mohamad AB, Takriff MS (2010) Experimental and theoretical study on the inhibition performance of triazole compounds for mild steel corrosion. *Corros Sci* 52:3331. <https://doi.org/10.1016/j.corsci.2010.06.002>
124. Lukovits I, Lalman E, Zucchi F (2001) Corrosion inhibitors—correlation between electronic structure and efficiency. *Corrosion* 57:3–8. <https://doi.org/10.5006/1.3290328>
125. Zhang W, Liu Y, Zhang Y, Wang L-J, Wu Y-C, Li H-J (2020) 9-Substituted acridines as effective corrosion inhibitors for mild steel: electrochemical, surface morphology, and computational studies. *New J Chem* 44:6464–6474. <https://doi.org/10.1039/d0nj00440e>
126. Boughoues Y, Benamir M, Messaadi L, Bouider N, Abdelaziz S (2020) Experimental and theoretical investigations of four amine derivatives as effective corrosion inhibitors for mild steel in HCl medium. *RSC Adv* 10:24145–24158. <https://doi.org/10.1039/d0ra03560b>
127. Qiang Y, Zhang S, Tan B, Chen S (2018) Evaluation of Ginkgo leaf extract as an eco-friendly corrosion inhibitor of X70 steel in HCl solution. *Corros Sci* 133:6–16. <https://doi.org/10.1016/j.corsci.2018.01.008>
128. Shalabi K, Abdallah YM, Hassan HM, Fouda AS (2014) Adsorption and corrosion inhibition of *Atropa belladonna* extract on carbon steel in 1 M HCl solution. *Int J Electrochem Sci* 9:1468–1487
129. Cerny V (1985) Thermodynamical approach to the traveling salesman problem: an efficient simulation algorithm. *J Optim Theor Appl* 45:41–55
130. Dagdag O, Safi Z, Erramli H, Cherkaoui O, Wazzan N, Guo L, Verma C, Ebenso E, El Harfia A (2019) Adsorption and anticorrosive behavior of aromatic epoxy monomers on carbon steel corrosion in acidic solution: computational studies and sustained experimental studies. *RSC Adv* 9:14782–14796. <https://doi.org/10.1039/c9ra01672d>
131. Fouda AS, Shalabi K, Idress AA (2015) *Cerantonia siliqua* extract as a green corrosion inhibitor for copper and brass in nitric acid solutions. *Green Chem Lett Rev* 8:17–29. <https://doi.org/10.1080/17518253.2015.1073797>
132. Qiang Y, Zhang S, Xu S, Li W (2016) Experimental and theoretical studies on the corrosion inhibition of copper by two indazole derivatives in 3.0% NaCl solution. *J Colloid Interfaces Sci* 472:52–59. <https://doi.org/10.1016/j.jcis.2016.03.023>
133. Qiang Y, Zhang S, Guo L, Xu S, Feng L, Obot IB, Chen S (2017) Sodium dodecyl benzene sulfonate as a sustainable inhibitor for zinc corrosion in 26% NH<sub>4</sub>Cl solution. *J Clean Prod* 152:17–25. <https://doi.org/10.1016/j.jclepro.2017.03.104>
134. Wang J, Qiang Y, Jiang L, Xiang B, Chen S, Xing S, Wang Y, Wang Y (2018) Excellent inhibition performance of low-toxicity dibenzylthiocarbamic acid zinc salt selfassemble nano-film for copper corrosion in sulfuric acid. *J Mol Liq* 271:959–969. <https://doi.org/10.1016/j.molliq.2018.09.061>
135. Putilova IN, Balezin SA, Barannik VP (1960) Corrosion inhibitors. Pergamum Press, Oxford, p 85
136. Evans UR (1990) The corrosion and oxidation of metals. Edward Arnold, London, pp 324, 326
137. Shams El Din AM, Fakhr MY (1974) A thermometric study of the reaction between Fe and HNO<sub>3</sub>. *Corros Sci* 14:635–644
138. Ellingham HJT (1932) *J Chem Soc* 15:65
139. Balezin SA, Parfenov GP (1953) *Russ J Appl Chem* 26:795
140. Benahmed M, Djeddi N, Akkal S, Laouer H (2016) *Saccocallyx satureioides* as corrosion inhibitor for carbon steel in acid solution. *Int J Ind Chem* 7:109–120. <https://doi.org/10.1007/s40090-016-0082-z>
141. Deng S, Li X (2012) Inhibition by Ginkgo leaves extract of the corrosion of steel in HCl and H<sub>2</sub>SO<sub>4</sub> solutions. *Corros Sci* 55:407. <https://doi.org/10.1186/1752-153X-7-83>
142. Baeza H, Guzman M, Ortega P, Vera L (2003) Corrosion inhibition of copper in 0.5 M hydrochloric acid by 1,2,3-thiadiazole-2,5-dithiol. *J Chil Chem Soc* 48:717–732. <https://doi.org/10.4067/S0717-97072003000300004>
143. Tan B, Zhang S, Liu H, Qiang Y, Li W, Guo L, Chen S (2019) Insights into the inhibition mechanism of three 5-phenyltetrazole derivatives for copper corrosion in sulfuric acid medium via experimental and DFT methods. *J Taiwan Inst Chem Eng* 102:424–437. <https://doi.org/10.1016/j.jtice.2019.06.005>
144. Karthik G, Sundaravadivelu M (2016) Investigations of the inhibition of copper corrosion in nitric acid solutions by levetiracetam drug. *Egypt J Pet* 25:481–493. <https://doi.org/10.1016/j.ejpe.2015.10.009>
145. Fouda AS, Ismael MA, AboShahba RM, Kamel LA, El-Nagggar AA (2017) Corrosion inhibition of copper and  $\alpha$ -brass in 1 M HNO<sub>3</sub> solution using new aryl pyrimido [5, 4-c] quinoline-2,4-dione derivative. *Int J Electrochem Sci* 12:3361–3384. <https://doi.org/10.20964/2017.04.57>

**Publisher's Note** Springer Nature remains neutral with regard to jurisdictional claims in published maps and institutional affiliations.